D1.1: State of the Art Review

Project number
313238

Project title
LOTUS— Preparing Land and Ocean Take Up from Sentinel-3

Call (part) identifier
FP7-SPACE-2012-1

Funding scheme
Collaborative project

Deliverable Number D1.1
Title: “State of the Art Review”
Nature: Report
Dissemination level: Public

Status: Draft
Date: 25 Oct. 2013.

DOCUMENT CHANGE LOG				
Rev.	Date	Sections modified	Comments	Changed by
1	2013-06-19	All	Draft submitted to DTU	Alejandro Egido
2	2013-10-25	All	Final Version	Alejandro Egido

Abstract

The current document provides a state of the art review for the processing of SAR mode data over the ocean. The document is structured according to the different sub-themes, i.e., Open Ocean, coastal zone, and polar ocean. In addition to the processing techniques, a review of the available corrections has been carried out to identify the most relevant ancillary information in order to derive meaningful geophysical parameters for each of the different sub-themes.

2. Basic Concepts of Radar Altimetry

This section provides the basis for the understanding of conventional and SAR Altimetry concepts. The section is based on Chapter 2 of the document (SAMOSA Team 2008), prepared by Starlab within the frame of the SAMOSA contract.

2.1. Radar Altimetry Concept

In the introduction of this technical note, radar altimetry has been described as the measurement of the time t_d of a radio signal to travel from the emitting instrument, reach a target surface, and return/scatter back. Altimetric measurements allow the detection of physical parameters hereafter listed:

- **Range:** distance from the satellite's centre mass to the sea surface $t_d = \frac{2R}{c}$ (c = speed of light) (needs atmospheric, sea-state corrections, etc.)
- **Significant wave height (SWH):** "*is the average height (through to crest) of the 1/3 largest waves*". Essentially, this is 4 times the standard deviation of the surface. Measurable from the skewness of the waveforms.
- **Wind Speed**

Observation geometries of conventional altimeters are essentially in a nadir looking angle.

Figure 1 provides an example of conventional pulse limited altimetry geometry. Radar altimetry measurements can be achieved using different emission types: mono pulse or burst of pulses, continuous emission, dual frequency emissions, etc. For this technical note, and in order to introduce the SAR Altimetry mode presented in the following chapter, this section only describes a single frequency system emitting a burst of pulses.

Previous to the analysis of the echo return from a burst of pulses it is convenient to introduce the echo return of a single emitted pulse.

Figure 2 a) shows the propagation of a single pulse along the beam of the antenna in the (z,y) plane, corresponding to a flat surface. The curved lines represent the pulse propagating and the temporal width between curves is meant to be constant and equal to τ_p, the pulse length in time. A different visualization of the propagation (looking down at the scattering surface from the instrument position) is provided in Figure 2 b). At the time the pulse reaches the observed surface, and until all the width of the pulse is in contact with the surface, the area illuminated by the emitted pulse will be defined by a circle, as the pulse propagates the circle transforms into rings of equal area (Fu and A.Cazenave 2001).

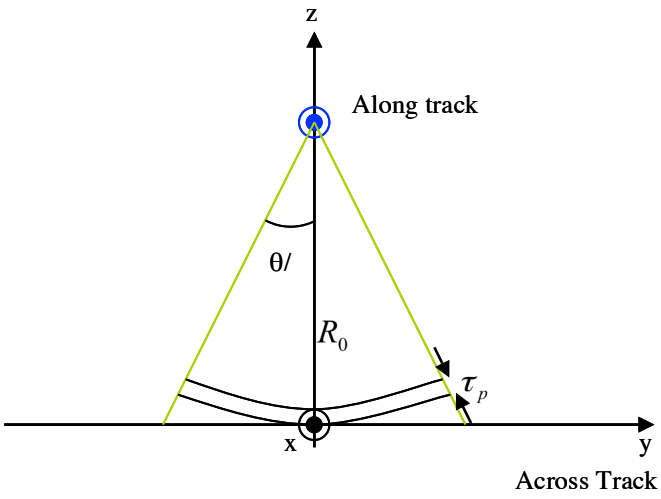

Figure 1: Conventional Altimetry observation geometry. τ_p = pulse length

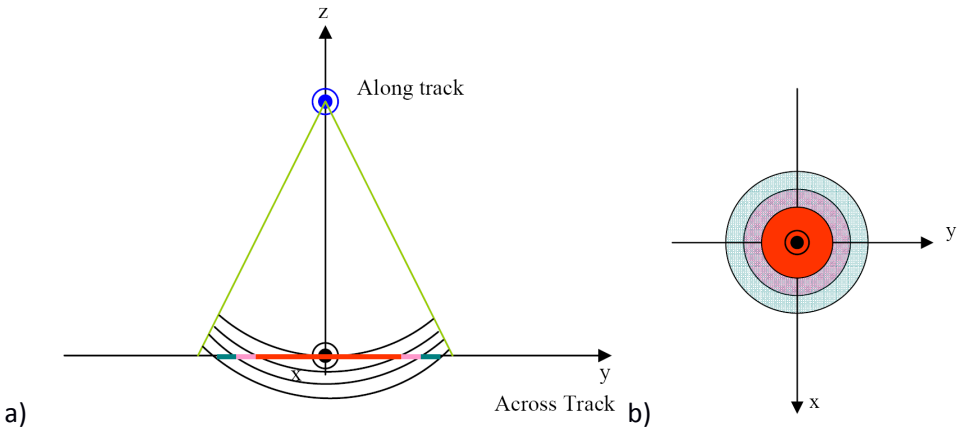

Figure 2: Mono Frequency – mono pulse system; a) Measurement geometry, b) surface footprint

With no further information, Figure 2 b) could lead to conclude that all the scattering contributions from the points within the same circle or rings may not be distinguishable given that they will be received simultaneously. However, this only applies if sensor and target are static, which is not the case in our geometry. Due to the sensor movement, airborne or satellite altimetry is also affected by the Doppler effect, hereafter described.

2.2. Doppler Effect in Radar altimetry

The relative motion between the observing sensor and the target, in radar observations results into an effect known as the Doppler effect.

Assuming a static observer and a moving target, Figure 3 displays the emission of two pulses at a time distance T_0. The time for the fist pulse to reach the moving target is t_1, the time for the second emitted pulse to reach the target is t_2. Due to the target motion, the first pulse will reach the target at a distance R_1, but the second emitted pulse will reach the target at a larger distance R_2.

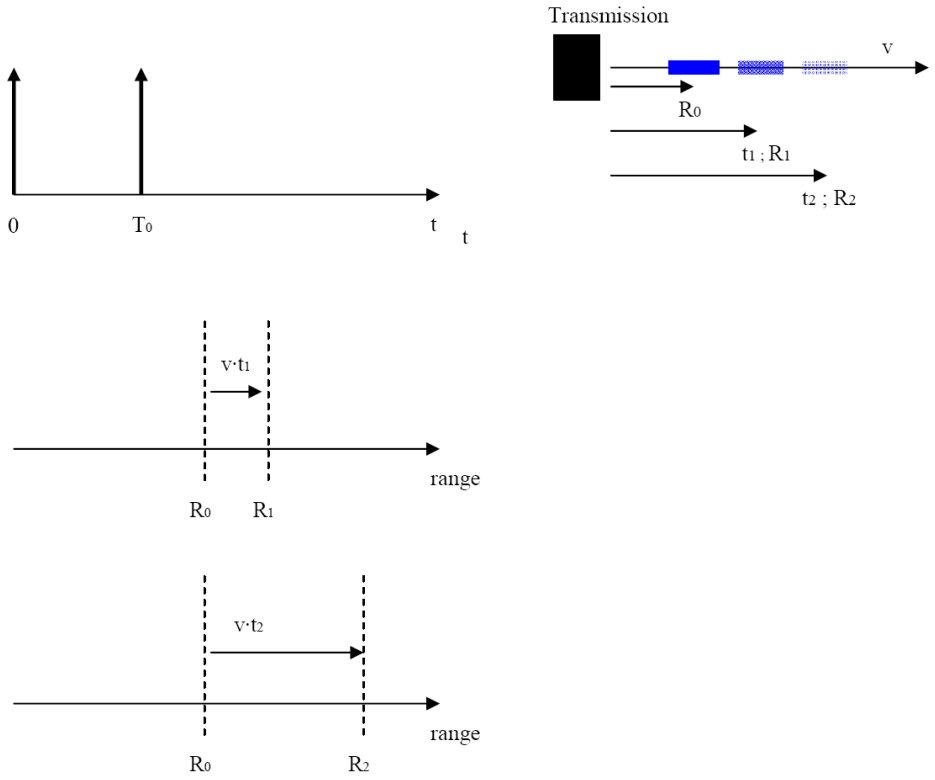

Figure 3: Doppler effect of a moving target

The difference in reception times of the two echoes can be related to frequency changes by:

$$f_r = \frac{1}{t_2 - t_1} = \frac{(c-v)}{(c+v)} \cdot \frac{1}{T} = \frac{(c-v)}{(c+v)} f_0. \qquad (3)$$

We refer to the difference of the previous frequency and the original emission rate ($f_0 = \frac{1}{T_0}$) as Doppler frequency.

$$f_D = f_r - f_0 \approx -2\frac{vf_0}{c}. \qquad (4)$$

for $c >> v$ (non-relativistic)

Given the previous, and considering the observation geometries in Figure 1 and Figure 2 all the contributions from the same ring will not have the same Doppler frequency. Therefore, the footprint view will be modified as presented in Figure 4.

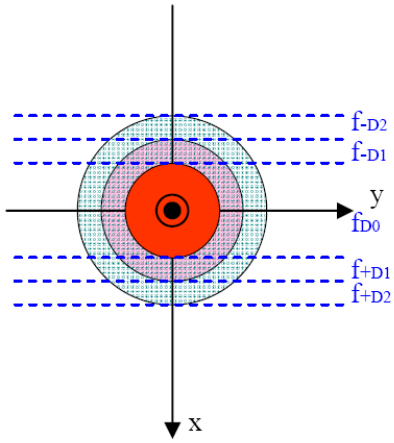

Figure 4: Doppler frequency map

Considering the Doppler effect, the contributions from the same ring in the along track direction will be distinguishable. On the contrary, the contributions from the same ring in the across track direction will be received simultaneously and will not be separable.

2.3. Radar Altimetry burst of pulses

Conventional altimeters usually emit a burst of pulses which observe the same footprint. This will result into more looks of the same footprint, thus will reduce the speckle noise effect. Pulse to pulse coherence is neither necessary nor desirable in conventional altimetry because incoherent, de-correlated averaging is needed for speckle reduction.

2.4. Conventional Altimetry Block diagram

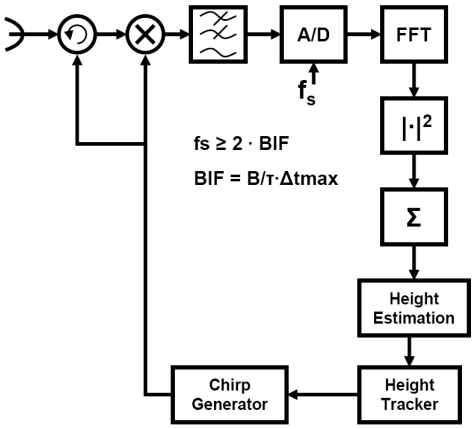

Figure 5: Conventional Altimetry Block diagram

Figure 5 shows a conventional altimeter block diagram. The first blocks have been already described in the previous section. Only the height estimation and height tracker have not been analyzed in this document yet. Both blocks are dependent on the final normalized power echo, which is described in the following section.

2.4.1. Return mean echo over ocean

This section will provide a more detailed description of the mean average impulse response of open Ocean, coastal areas, and in land water surfaces. This section is only meant to introduce the rough surface response for the better understanding of the diagram block, specially height estimation and height tracker.

Previous studies have demonstrated that the impulse response of an ocean surface can be represented as follows (Brown 1977):

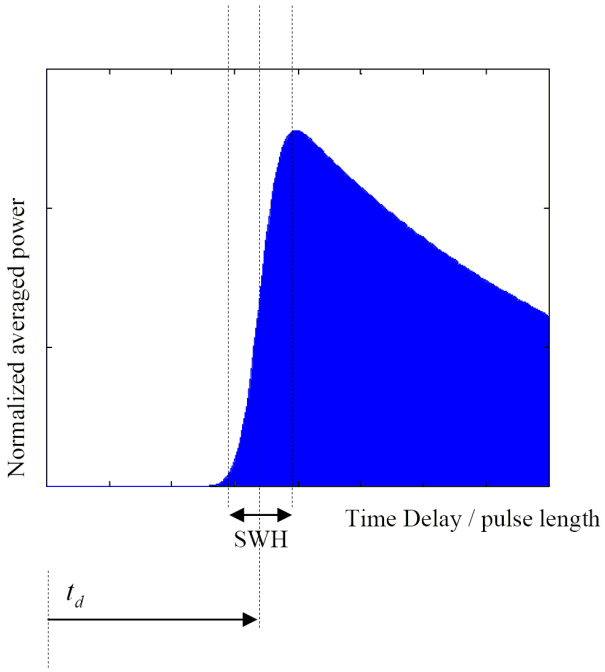

Figure 6: Shape of a returned normalized echo power. In blue σ_0

Figure 6 illustrates the return normalized echo power of a single emitted pulse. From the figure a rise region and a trailing edge region can be identified. The time delay, the SWH and the wind speed (dependent on the RCS) as illustrated in Figure 6 can be measurable from the impulse response.

2.5. SAR Altimetry

SAR altimetry was first described as Delay/Doppler Radar Altimetry in (K. Raney 1998). In this section, the terms Delay/Doppler Radar altimetry and SAR altimetry are used indistinctly. The key innovation of SAR altimetry is the addition of along track processing for increased resolution and multi-look processing. This technique requires echo delay compensation, analogous to range cell migration correction in conventional but unfocused SAR. Due to this innovation, spatial resolution is increased in the along-track dimension and Delay/Doppler mapping is provided. In turn, this allows for accumulation of equivalent looks of a scattering area, leading to speckle reduction and altimetric performance. This section describes SAR altimetry mode, SAR geometry, Delay/Doppler concept, and the performance of SAR Altimetry versus conventional altimetry will be detailed.

2.5.1. SAR Observation Geometry

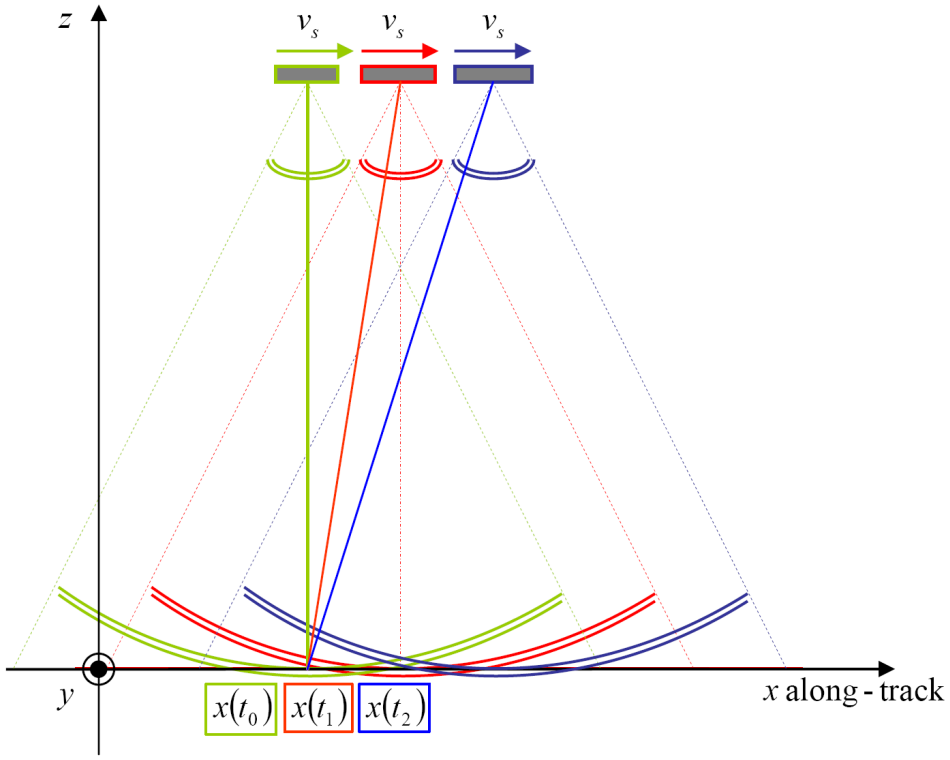

Figure 7: SAR Observation geometry of a scattering point

SAR altimetry processes the data such that they could be seen as been acquired from a synthetic aperture antenna. Thus, the contribution from a scattering point will be distinguishable as the airborne or satellite moves. Figure 7 shows the observation geometry of a scattering point in SAR Altimetry mode. Differently to conventional altimeters, SAR altimeters use most of the power received, in fact in conventional altimetry the power contribution of the adjacent scattering points to the one of interest is lost.

2.5.2. SAR Altimetry Concept

Delay/Doppler radar altimetry benefits from the conventional pulse compression in the range dimension. Additionally, SAR altimetry introduces along-track processing for azimuth mapping. The main requirement for the use of the SAR processing in altimetry is the coherency within each burst of pulses (K. Raney 1998) which differs from conventional altimetry. The basic processing steps of the SAR altimeter are depicted in Figure 8. Note that this is a simplified block diagram intended for conceptual algorithm representation, i.e. it is not Hardware (HW)/Software(SW) optimized.

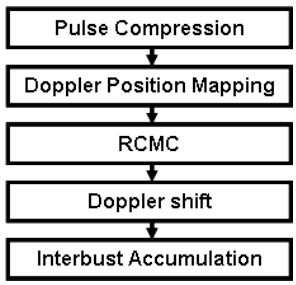

Figure 8: Basic steps of the SAR altimeter processing

The delay/Doppler altimeter, just as with a conventional altimeter, uses pulse compression in the range dimension. The range signal, a frequency modulated pulse or Chirp, is multiplied by a delayed replica of the transmitted signal, low pass filtered and compressed by means of an FFT. The range-compressed echoes are stored in the “slow-time” or along-track dimension resulting in a 2D data matrix. In addition, an along-track FFT is applied to the data in order to map the Doppler frequency of each echo. The Doppler frequency is related to the relative position of the scatter with respect to the movement of the satellite. The known position of the scatter delay time correction is applied to each Doppler bin. Next to the compensation, the range position (i.e. delay time) of each scatterer over its entire illumination history is equal to its minimum range; this process is applied burst-by-burst. The Doppler shift is performed in order to place the information of each scatter, distributed in different bursts at different Doppler bins, in the same Doppler bin. The previous process facilitates the average waveform retrieval. Using SAR Altimetry the contribution of adjacent scatters will be effectively minimized, and the desired scatter contribution maximized for each computed waveform. Note that the influence of adjacent targets in the final waveform depends on impulse response of the system.

2.5.3. Pulse Compression

Delay/Doppler radar altimeters use the same pulse compression in range dimension, as conventional incoherent radar altimeters.

2.5.4. Doppler Position Mapping

The Doppler position mapping refers to the Fourier transform of the 2D data matrix in along-track direction. Subsequently to this operation, the information of the different scatters is redistributed depending on their relative position with respect to the motion of the satellite.

The Doppler spectrum has a geometric interpretation. The Doppler frequency is given by the dot product of the pointing or observation unit vector (depending on observation angle) and the spacecraft velocity vector. Therefore, there is a unique correspondence between the observed Doppler frequency f_D and the observation angle θ_i of the scatter.

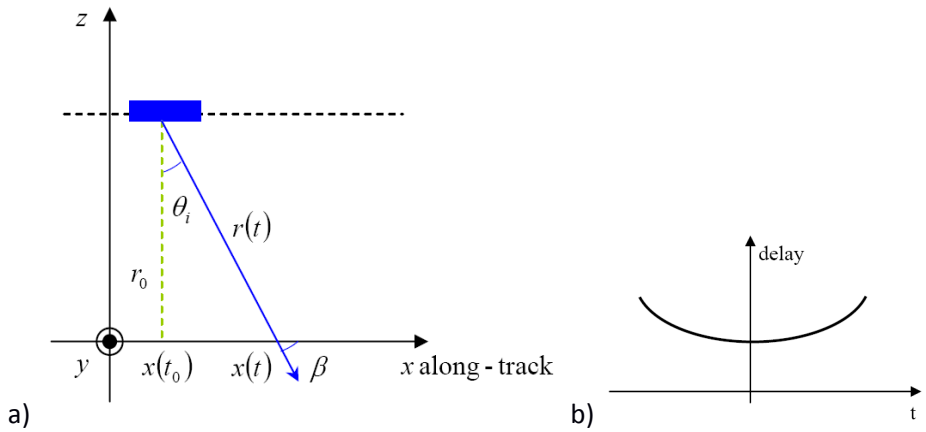

Figure 9: a) Along-track scattering point observation; b) Doppler Spectrum geometry

In a simple form, the Doppler frequency can be written as:

$$f_D(\theta_i) = \frac{2}{\lambda} \cdot (\vec{p} \cdot \vec{v}_S) = \frac{2 \cdot v_S \cdot \cos(\beta)}{\lambda} = \frac{2 \cdot v_S \cdot \sin(\theta_i)}{\lambda} \quad (8)$$

being v_S is the spacecraft velocity. For the range variation ($r(t)$) with respect to the observation angle (again in a simple geometry) applies

$$(x_t - x_0) \approx r(t) \cdot \sin(\theta_i). \quad (9)$$

Therefore, the Doppler frequency can be approximated as

$$f_D \approx \frac{2 \cdot v_S}{\lambda} \cdot \frac{\left(x(t) - x(t_0)\right)}{r(t)}. \qquad (10)$$

The position of a scatterer through the time *r(t)* and Doppler frequency *R(f)* follows a hyperbolic law which is known as range cell migration.

$$r(t) = \sqrt{r_0^2 + v_S^2 \cdot (t - t_0)^2}, \qquad (11)$$

where r_0 is the minimum slant range of the satellite to the scatterer, satellite height in this case, and $t_0 \approx x_0 / v_B$ (v_B is velocity of the altimeter's antenna illumination along the terrain) the corresponding over flight time.

Therefore, each Doppler bin represents a unique along-track position of a scatterer.

2.5.5. Range Cell Migration Correction

The correction of the range cell migration is necessary in order to place all observations of a scatterer at the same radar range. The relative delay δt of a given scatterer can be derived form Equation [11] as follows:

$$\delta(t) = r(t) - r_0 = r_0 \cdot \left[\sqrt{1 + \alpha \cdot \frac{(x - x_0)^2}{r_0^2}} - 1 \right], \qquad (12)$$

Being the orbital factor $\alpha = V_S / V_B$. After some manipulation and the expansion of the square root in Taylor series, the next simplified expression is obtained[1],

$$\delta(t) \approx \frac{\alpha}{2 \cdot r_0} \cdot (x - x_0)^2. \qquad (13)$$

This factor is applied to each Doppler bin for the range cell migration correction (RCMC). Note that the RCMC shall be applied in the Doppler domain. In this domain, all Doppler bins should be corrected by the same delay.

2.5.6. Doppler Shift

At this stage, the range migration has been compensated. However, the information from a scatterer still remains at a different Doppler bin for each processed burst. A Doppler shift places the information of a scatterer in the same Doppler bin allowing for unfocussed SAR processing.

[1] Note that the orbital velocity factor should be squared in contrast to (K. Raney 1998).

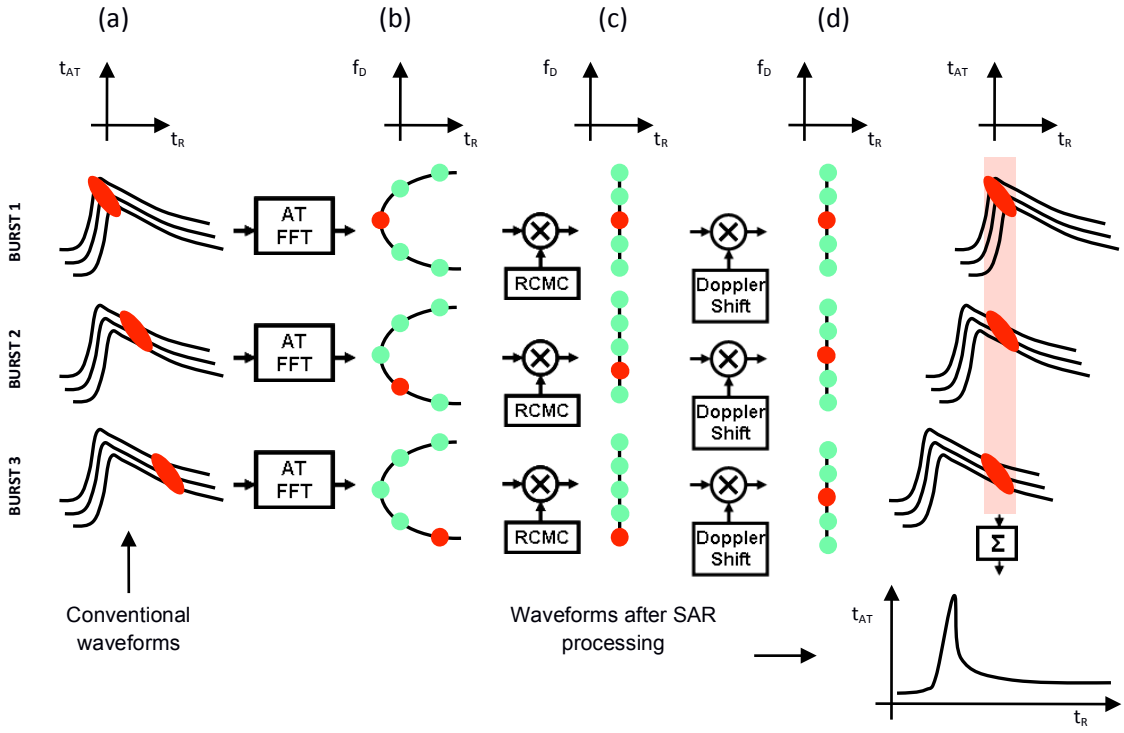

Figure 10: SAR altimetry diagram block representation. (a) Waveforms after range compression. (b) After along-track FFT, the scatterer's returns are placed in a Doppler bin (points) depending on relative position to spacecraft. (c) Compensation of delay due to range cell migration. (d) Doppler shifted bins before detection and accumulation. Note that the domain of the different plots is represented in the upper part of the picture where t_{AT} is along-track time, t_R range time and f_D Doppler frequency. The red points represent the information of the same scatterer through the whole processing chain.

2.5.7. Inter-burst (incoherent) Accumulation

In conventional altimetry within each burst there will be several looks (one per pulse within the burst). SAR altimetry also maintains the previous looks, and due to its along-track geometry this technique will add additional looks with respect to a conventional altimeter, since the scatterer will be visible in different subsequent bursts.

Using the Doppler shift the along-track looks will be detected, accumulated and averaged to reduce speckle noise effects. The information from a scatterer after averaging will transform into a sharp waveform as in Figure 11. Note that the along-track accumulation corresponds to an unfocussed SAR compression, i.e. the Doppler phase modulation due to the movement of the platform has not been compensated.

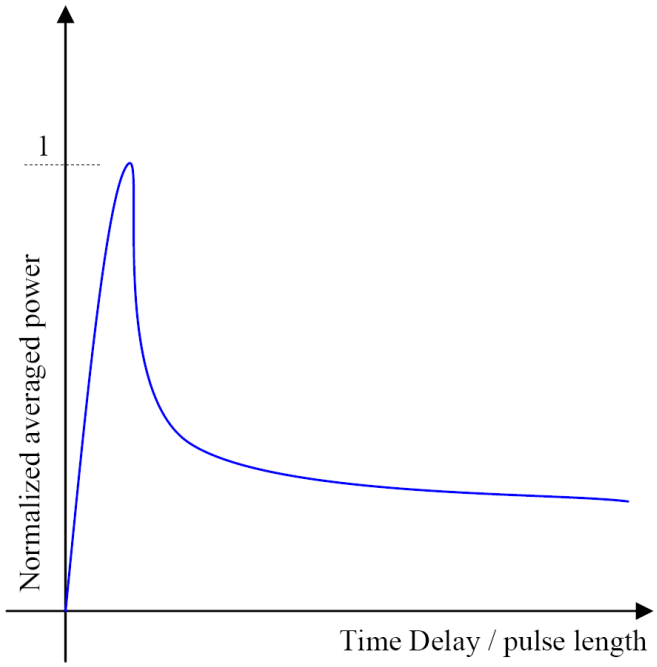

Figure 11: Normalized Average power. Image acquired (K. Raney 1998).

2.5.8. SAR Altimeter block diagram

Figure 12 reproduces the delay/Doppler altimeter block diagram (block based in (K. Raney 1998)). The new blocks with respect are highlighted in blue.

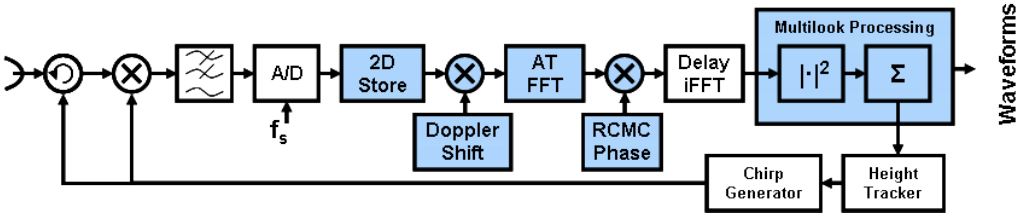

Figure 12: Delay/Doppler Altimetry Block diagram.

Note that Doppler shift is performed by multiplication of the along track lines with a constant phase factor in the delay/along-track domain based on Fourier theory. After the along-track FFT, the range cell migration compensation (RCMC) is carried out by multiplication of the range lines with a constant phase factor in the delay-Doppler domain. Finally, after the completion of the range compression, the Doppler bins coming from different burst are detected and averaged for SNR optimization.

2.6. SAR Altimetry Performance vs. Conventional Altimetry

SAR altimetry, contrarily to conventional altimetry is not pulse limited, but beam limited. In essence SAR Altimetry benefits from all the data within the 3dB antenna pattern. This result into an increment of the integration time, i.e. of the signal power processed even though the post-processing along-track size is smaller.

2.6.1. Signal-to-noise ratio

The SNR of the delay/Doppler altimeter is increased by the contribution of the complete antenna pattern in along-track. In across-track, the pulse length remains as upper threshold of the range integration time.

The SNR of a pulse compressed radar is given by:

$$SNR = \frac{P_T \cdot G^2(\xi) \cdot \lambda^2 \cdot C_R \cdot \sigma^0 \cdot A_\sigma}{(4\pi)^3 \cdot r(t)^4 \cdot N} \qquad (14)$$

where P_T is the transmitted power, G the antenna gain, λ the wavelength, C_R the range compression factor or time bandwidth product, σ^0 the sigma nought, A_σ area of the resolved footprint, r the slant range distance to the scatter or satellite height h in this case, and N the noise power.

Assuming that both altimeters have identical system parameters, the only difference in SNR of a pulse-limited altimeter and a SAR altimeter is the area of the resolved footprint.

The area of the footprint for the pulse-limited altimeter is given by (K. Raney 1998):

$$A_{PL} = \frac{\pi \cdot c \cdot \tau_p \cdot h}{\alpha} \qquad (15)$$

Being τ_p the transmitted FM pulse length and α the orbital velocity factor. This is basically of the form $A_{PL} = \pi \cdot R^2$, with R the limiting circle for a quasi flat surface response function on a spherical earth associated to the pulse length. Note that slant range to the scatterer r has been substituted by the satellite height h.

In addition, the area of the footprint for a delay-Doppler altimeter is given by (K. Raney 1998):

$$A_{DD} = 2 \cdot h \cdot \beta \cdot \sqrt{c \cdot \tau_p \cdot h \cdot \alpha} \qquad (16)$$

being β the along-track antenna beamwidth. This is basically ADD = 2·R·β·h essentially, data and power are collected during the entire time the observation cell is visible by the antenna. This is the crucial difference from conventional altimetry.

Considering the previous equations, the improvement in terms of SNR is directly dependent on the footprint areas for each altimetry concept.

$$\Delta SNR = \frac{A_{DD}}{A_{PL}} = \frac{2\beta}{\pi} \cdot \sqrt{\frac{h \cdot \alpha^3}{c \cdot \tau_p}} \,. \qquad (17)$$

2.6.2. Footprint

In contrast to conventional altimeters a SAR altimeter has two independent dimensions: along-track and across-track (range). After SAR processing, these two variables describe an orthonormal data grid as shown in Figure 13.

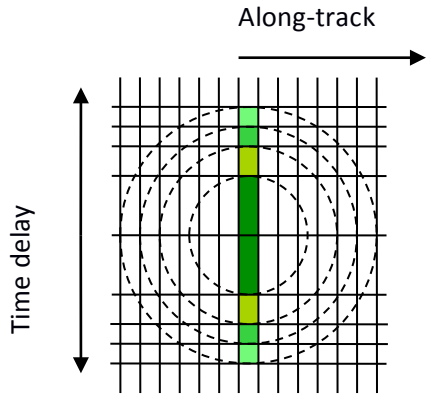

Figure 13: delay/Doppler altimeter footprint

The actual nadir point is located in the Doppler bin correspondent to zero Hertz and ideally, it is equivalent to along-track position of the satellite. Vertical spacecraft velocity will add Doppler shift to the signals, which should be compensated in order to avoid unwanted along-track shift of the data positions.

The Doppler frequency bin Δf_D is defined from the pulse repetition frequency PRF and the number of pulses per burst N_B

$$\Delta f_D = \frac{PRF}{N_B} \,. \qquad (18)$$

The along-track altimeter resolution Δx is determined by the scatter illumination time, i.e. the burst length τ_B; and it can be defined as,

$$\Delta x = \frac{v_B}{B_P} \qquad (19)$$

being v_B the velocity of the beam or footprint velocity, and B_P the equivalent Doppler bandwidth processed which can be defined under some considerations as:

$$B_P \approx k_R \cdot \tau_B \approx \frac{2 \cdot v_s^{\,2}}{\lambda \cdot h} \cdot \tau_B \qquad (20)$$

k_R is the Doppler rate, widely use in SAR processing. Therefore, the along-track resolution can be written as

$$\Delta x \approx \frac{v_B}{2 \cdot v_s^{\,2}} \cdot \frac{\lambda \cdot h}{\tau_B}. \qquad (21)$$

Assuming that $V_B = V_S$ and introducing the round-trip delay time T_R, the along-track resolution can be finally written as in [Ref 2]

$$\Delta x \approx \left(\frac{c \cdot \lambda}{4 \cdot v_s} \right) \cdot \frac{T_R}{\tau_B}. \qquad (22)$$

2.7. Summary of Characteristics of SAR vs. Conventional Altimetry

SAR mode altimetry offers the potential following improvements with respect to conventional altimetry:

- Increment of efficiency of height estimation
- Reduction of footprint dimension in along track
- Smoothed speckle noise with respect to conventional altimeters
- Increment of ca. 10 dB in signal to noise ratio (the delay/Doppler altimeter integrates much more instrument's radiated power).

Compared to conventional altimetry the improvement in SNR as well as to the new waveform model (Phalippou and Enjolras 2007), the minimum attainable range accuracy is higher. (Phalippou and Enjolras 2007) showed that the range accuracy is improved by a factor 2 upon conventional altimeter for a Poseidon class altimeter which is the one flown on satellites like Jason-1, Jason-2.

For Cryosat-2 and Sentinel-3 this range accuracy improvement is counter acted by the fact that in SAR mode the instrument is only measuring roughly 30 % of the time.

3. Open Ocean

The current section comprises a review of the SAR Altimetry technology status over Open Ocean, containing detailed analysis of the existing retracking models, their related limitations, drawbacks and challenges. This section reviews also the Reduced SAR (RD-SAR) processing technique that aims to reproduce Low Resolution Mode (LRM) data out of SAR data, with the purpose of ensuring continuity with the data of previously existing altimeters.

3.1. SAR Altimetry Technology Status and Perspectives

The Delay Doppler/SAR radar altimeter is a new generation of instrument allowing to provide unprecedented measurements of ocean parameters with noticeably higher precision and resolution capabilities than what is typically seen with conventional pulse limited altimeters. Given the high performance of this technique, several altimeter missions based on pulse-limited "conventional" instruments are progressively moving to the use of Doppler/SAR instruments. The Cryosat-2 mission is the first radar altimeter satellite to use this technique. It is currently operating in orbit for about 3 years. Initially devoted for cryosphere observations, the SAR mode capability of the CryoSat-2 SIRAL altimeter also presents the opportunity of demonstrating significant potential benefits of SAR altimetry for ocean applications, based on expected performance enhancements which include improved range precision and finer along track spatial resolution, as this mission provides also ocean data and about 12% of the open ocean is covered in SAR mode. This flight data set is of tremendous importance to assess the in orbit data quality of the SAR mode.

The next Doppler/SAR instrument will be onboard the Sentinel-3 mission and the envisaged Jason-CS mission. On Sentinel-3, ESA and the EC are expecting to use the SAR mode during the full satellite cycle, which will enable an unprecedented sampling of the ocean surface. Jason-CS is expected to operate in an interleaved mode that will allow to produce both SAR and LRM data. The launch for Sentinel-3 is expected for 2014/2015, whereas for Jason-CS the launch date is envisioned for 2017/2018. This ensures a long term the continuity of SAR altimetry products.

3.2. SAR Altimetry Retracking algorithms

Several studies have been initiated and are ongoing to develop and test the most suitable processing algorithms – in term of retracking - for this new altimeter mode, with the final objective to enhance the potential benefit of the SAR mode data over the ocean surface (there is also several studies ongoing for other surfaces types like inland water, coastal, …). This is of high importance for the Sentinel-3 mission and the expected Jason-CS mission. The exploitation of the Delay/Doppler altimeter oceanic information is based on the analysis of the reflected oceanic waveform. But this waveform has now a peaky shape that is different from the conventional altimetric echo. It may be interpreted as a change of illuminated geometry on sea surface from a "classical" surface-constant ring type to a fragment only of the ring area that is narrowed along the satellite track direction by the synthetic aperture processing (a few hundreds of meters in width in the along track direction). The pulse-limited classic altimetry model (Brown 1977) is no longer valid for a "beam-limited" altimeter that needs the development of a new altimetric signal model to fit the observed Doppler return waveforms.

As for conventional altimetry, the average backscattered power of a Doppler echo is derived via convolution of three terms: the flat sea surface response (FFSR), the sea wave height probability density function and the time/frequency pulse target response of the radar. Different waveform retracking techniques based on fitting this convolution model to the observed Doppler waveforms may be used. There are mainly 3 different approaches regarding the formulation of the model to retrack SAR data: 1) a solved analytical model with known derivatives of the model (e.g. Brown model), 2) a solved analytical model without formulated derivatives (for which the retracking employs numerical derivatives), and 3) an unsolved analytical model (computed by the double convolution operation).

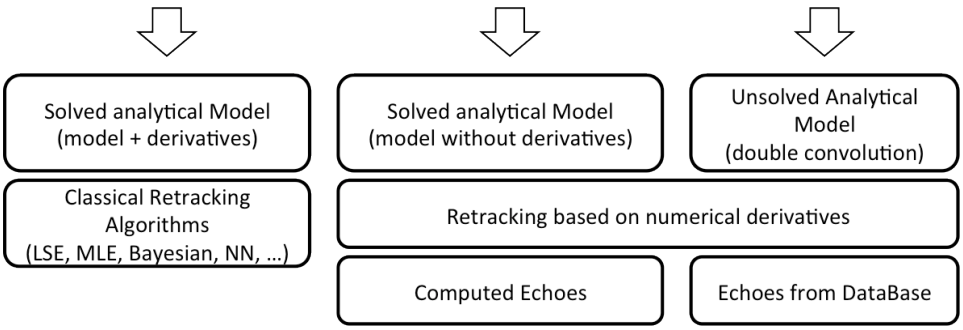

Figure 14: *Different echoes processing for geophysical parameter estimation*

Three different retracking schemes are discussed here. The first algorithm is based on a solved semi-analytical model (and the associated estimation algorithm). The second one consists in numerically simulating the Doppler echoes model (for unsolved analytical model). The third retracking scheme is based on the so-called SAMOSA model, which implements an analytical solution for the SAR waveforms.

3.2.1. A (semi-) analytical model for Doppler altimetry (Halimi, ENSEEIHT/Toulouse)

In the frame of a research project directed by CNES, CLS and the University of Toulouse, Halimi thesis study aims at developing an analytical modeling of the SAR altimeter ocean power-waveform, and an associated retracking algorithm to infer the sea surface parameters (i.e. epoch, wave height and amplitude).

Starting from the same hypotheses made by Brown, but using a different geometrical approach, an analytical formula for the FSSR associated with Doppler altimetry has been derived (A. Halimi 2012). The proposed FSSR model includes earth roundness, considers a Gaussian approximation for the antenna gain as it is used in the classical Brown model, and it doesn't contain antenna mispointing angles. The double convolution defining the mean power is then computed numerically. In this operation a cardinal sine function is used to model the PTRs in along-track and across-track directions. In some situation, the use of the real shape of the PTRs may be preferred to handle distortions. In this way, the power waveform avoids analytical approximation, minimizing the geophysical dependent biases in the retrieval parameters. The resulting single-look model depends on three parameters: the epoch, the sea surface wave height and the amplitude. A multi-look model is obtained by summing all

the reflected power from the along track beam surface of interest after applying appropriate delay compensation. A least squares approach based on the Levenberg-Marquardt algorithm is then applied to estimate the 3 parameters (i.e., epoch, the sea surface wave height and the amplitude) associated with the multi-look Doppler model.

Simulation results performed on synthetic data clearly show the potential of the SAR altimetry when compared to conventional altimetry in terms of error reduction. The analysis of real Cryosat-2 waveforms has confirmed the effective performance of the proposed Doppler model since a better estimate is obtained than with the usual conventional method. However, when dealing with antenna mispointing angles as encountered on-board Cryosat-2, this no-mispointing solution model is no longer well suited. The sensitivity of the SAR-mode altimeter data to off-nadir mispointing (mainly across-track) angle is known. It leads notably to errors in the retrieval. A new formulation of the SAR echo model with 5-parameters, including mispointing angles in across and along-track directions is currently under investigation in order to improve the consistency between the SAR altimeter waveform and model at varying parameters (particularly in different pointing scenarios).

3.2.2. A numerical retracking algorithm (CryoSat Processing Prototype, CNES/Toulouse)

Over the past 3 years CNES has set up a Cryosat Processing Prototype (CPP) to facilitate the development and testing of CNES innovative methods for processing SAR mode data over ocean. This prototype aims at contributing to expertise studies for the future Sentinel-3 mission. It was implemented in an attempt to provide very accurate and valuable data products that would permit the full exploitation of the capabilities of the Cryosat-2 SIRAL radar altimeter, and more globally assess the benefits of the SAR mode whose improvements have only been predicted in theory up to now. This investigation is also relevant for the specification of the SAR mode to be embarked on-board the Jason-CS mission. In addition, it addresses a number of questions relating to the SAR mode, such as the performance of the various retracking algorithms, the altimeter technologies (closed burst mode vs interleaved), the SAR mode retrievals sensitivity (to satellite pointing and directional waves), the Sea Surface Bias (SSB), and land contamination, to name a few. It is part of a challenging program led by operational and research agencies (ESA, EUMETSAT, NOAA, CNES and NASA) that are primarily concerned with meeting the future expectations of the scientists and operational users from the ocean community and other scientists interested in the remote sensing of sea-ice, land ice and hydrology.

Regarding the SAR-mode processing, a numerical retracking algorithm based on simulation of Doppler echoes model is implemented, (Deng 2003), (Boy, et al. 2012). The CPP SAR-mode retracking algorithm is a standard least squares estimator consisting in fitting a Doppler waveform with a multi-looked echo model that is pre-computed off-line by a simulator. The main innovation of this approach resides in the generation of the echo model database in which the sensitive parameters (sea-state, satellite parameters) vary, one parameter at a time, in a range of values and with a step size, that have been chosen to ensure the accuracy and precision of the estimates. This method may require huge data storage and, inevitably, long processing times, thereby suggesting some difficulties to cope with the implementation of this strategy, which should be considered in future or related work. However, this method is considered to be more robust than analytical ones, particularly when faced with atypical observations (e.g., elliptical antenna pattern, off-nadir mispointing angles, point target response) that

are difficult to put into equations. It was recently used to evaluate the Halimi semi-analytical approach by model comparison.

Multi-looked echo models are computed by using a simulator that mimics the Cryosat-2 altimeter response in SAR mode. This simulator consists of several components: 1) a scene generator module that generates a flat sea surface with high-resolution 1mx1m, 2) a power returns simulation: radar equation is applied to each point of the surface to compute the backscatter power taking into account the real elliptical antenna pattern. Signals in amplitude are then sorted by Doppler band and accumulated in the appropriate range gates of the waveforms. 3) The resulting model of the FSSR is convolved with the PTRs (in along-track and distance) of the radar. The Doppler bands corrected in range are then summed (multilooking) to finally form the Doppler echo model for a flat sea surface (the sea wave height is applied "on the fly" in the retracking process). This simulator has been validated by exhaustive testing (i.e., comparison between the estimated surface parameters and the initial ones with a LRM maximum likehood estimator).

As for conventional altimetry, the ocean parameters estimated from the numerical SAR retracking are expressed as:

$$\theta_n = \theta_{n-1} - g\left(BB^T\right)^{-1}_{\theta_{n-1}} (BD)_{\theta_{n-1}}$$

Where θ_n is the estimated parameter at iteration n; B,D are the partial derivatives and residuals matrix, and g is the loop gain (between 0 and 1).

For unsolved analytical model, derivatives of the mean return power can be computed numerically. The method consists in approximating the derivatives by a finite difference involving the database of pre-computed echo models. At each iteration n, models using the current estimation vector θ_{n-1} are directly taken from the database. The performances of this method have been evaluated theoretically using simulated LRM waveforms and, have been statistically validated on real data by applying it on J2 raw measurements. The results are found to be consistent with those obtained from a classical MLE4 retracking.

The numerical SAR retracking is based currently on a 3-parameters model that accounts for varying off-nadir mispointing angles provided by the star trackers. First results (focusing on the range and so on the epoch) have been assessed through Cal/Val process and recently communicated to scientific meetings. Analyses of sensitivities of this solution are still under study.

3.2.3. A numerical retracking algorithm (CLS/Toulouse)

CLS has been conducting different studies, on CNES funding, to better understand the principle of the SAR processing and to develop simulation tools that are able to exactly reproduce the raw echoes acquired by a SAR mode altimeter and to process them, accounting for all corrections up to the final retracking algorithm. Based on an end-to-end SAR radar altimeter simulator, CLS has developed its own SAR numerical retracking. The proposed technique slightly differs from the CPP one. The main difference resides in the construction of the echo model database. On CNES side the database is generated by an amplitude numerical simulator method and on CLS side by a complex numerical

simulator method that applies the usual Doppler processing scheme and the multilooking step. The present Doppler/SAR echo model is not taking into account for mispointing angles in the solution process as well.

The SAR numerical retracking algorithm is similar to the CPP one as discussed previously. However extra computing effort is done to simulate all pulses contributing to a Doppler echo and to average hundreds of incoherent Doppler/SAR waveforms to remove the speckle noise and obtain proper smoothed model echo. It makes the method time-consuming and more complicated to implement.

This algorithm including the true Doppler processing has been served as a reference, and has already provided a substantial support to the development of the operating CNES CRYOSAT Processing Prototype (CPP). Some evolutions of the model are already planned to better account for the effects of new parameters (radial velocity, altitude and antenna mispointing angles) and lead to a model that will therefore be more representative of Cryosat-2 SAR altimeter measurements.

3.2.4. Semi-analytical SAR waveform model

(Wingham, Phalippou, et al. 2004, Giles, et al. 2012) proposed a semi-analytical solution to the radar equation. The model has been implemented at UCL and the expression of the model is summarized in Figure 15, (Giles, et al. 2012).

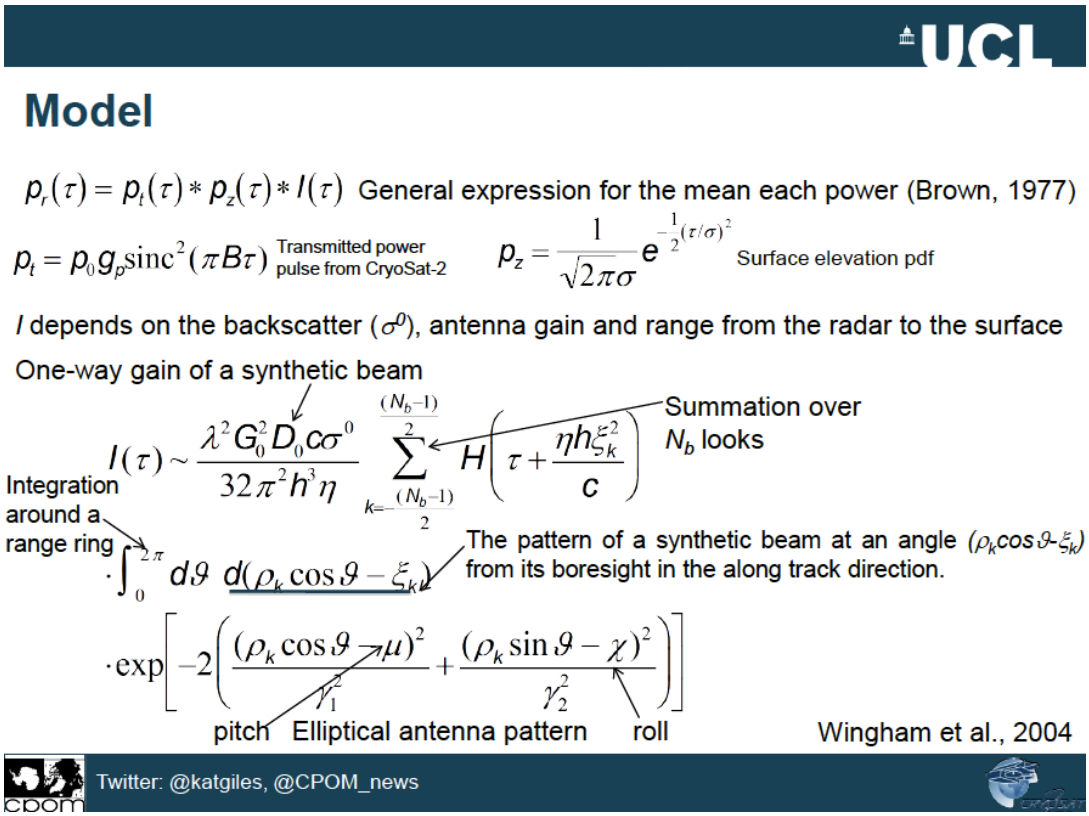

Figure 15: Figure 15: Formulation of the semi-analytiucal SAR waveform model developed by UCL from (Giles, et al. 2012).

The model accounts for the slight ellipticity of the CryoSat-2 antenna beam and shows explicit dependence of the SAR waveforms on platform roll and pitch mispointing angles.

3.2.5. Analytical retracking algorithm (The SAMOSA Model)

In the context of the Contract Change Note to the SAMOSA contract (ESRIN Contract 20698/07/I-LG) the algorithms and software specifications for the retracking of SAR altimeter ocean waveforms has been defined in (Ray and Martin-Puig 2012).

The detailed processing steps for the SAR waveform fitting is based on the prototype SAR retracker developed in SAMOSA, which uses un-weighted non-linear least-square fitting and does not require the explicit knowledge of the partial derivatives of the fitted model. As stated previously, it would take considerable effort to produce analytical formulas of the first order derivatives of the multi-looked SAR waveform model.

The SAMOSA project defined two waveform models. One accounting for: Gaussian ocean statistics, along-track curvature effects only, along-track mispointing angle effects, and circular antenna pattern. This model is referred as the SAMOSA1 waveform model. Moreover, the SAMOSA1 model was upgraded to the SAMOSA2 waveform model which accounts for Non-Gaussian Ocean statistics, curvature effects along and across-track, mispointing effects along and across track, radial velocity effects and elliptical antenna pattern. Both retrackers were evaluated with CRYMPS and CryoSat-2 data. SAMOSA1 waveform model applied to CRYMPS data and compared to RDSAR retracked data was shown to offer almost two-fold improvement in the range retrieval. Although SWH retrieved values are worst than in conventional altimetry for CRYMPS data. The SAMOSA 1 retracker performance was also evaluated with ASIRAS data resulting in a successful fit for more than 96% of the waveforms when ASIRAS is configured to have 64 pulses per burst and a maximal look angle of 1.4 degrees. SAMOSA-2 waveform model is more complex and requires further computation time than the SAMOSA-1 model. This has also been applied to CRYMPS data and the results confirm the same as its predecessor.

The SAMOSA-3 model is a further development on the SAR-Altimetry modelling, aimed at overcoming the computation time limitation of the previous SAMOSA models. These improvements are sought in computational time in the usage of the waveform model for altimeter data retracking. In essence, SAMOSA-3 is an analytical derivation of SAMOSA-2 as an expansion in a set of basis functions and a truncation of the final expression, in order to keep the most important terms in the expansion. The implementation of the basis functions was done in Look-Up Tables (LUTs) in order to improve the computational speed. During the SAMOSA-3 project, it was verified that the relative error of the truncated analytical expression with respect to the full-waveform model was below 1%, (Ray and Martin-Puig 2012). The SAMOSA-3 model was therefore considered suitable for the retracking of CryoSat-2 SAR mode data over the ocean.

3.2.6. Empirical SAR waveform model

An empirical fully-analytical model was proposed by (Sandwell, Garcia and Smith 2011) for the purpose of retracking CryoSat-2 SAR waveforms for improved marine gravity. The proposed formulation is shown in Figure 16. While the formulation is indeed simple, it is not clear how/whether the empirical model captures the effect of the asymmetric antenna pattern and the influence of mispointing. The 20Hz range noise obtained for CryoSat-2 SAR data with this empirical model was found to be larger than that observed by other groups, leading the authors to conclude that this "fully-analytic retracking model is suboptimal"

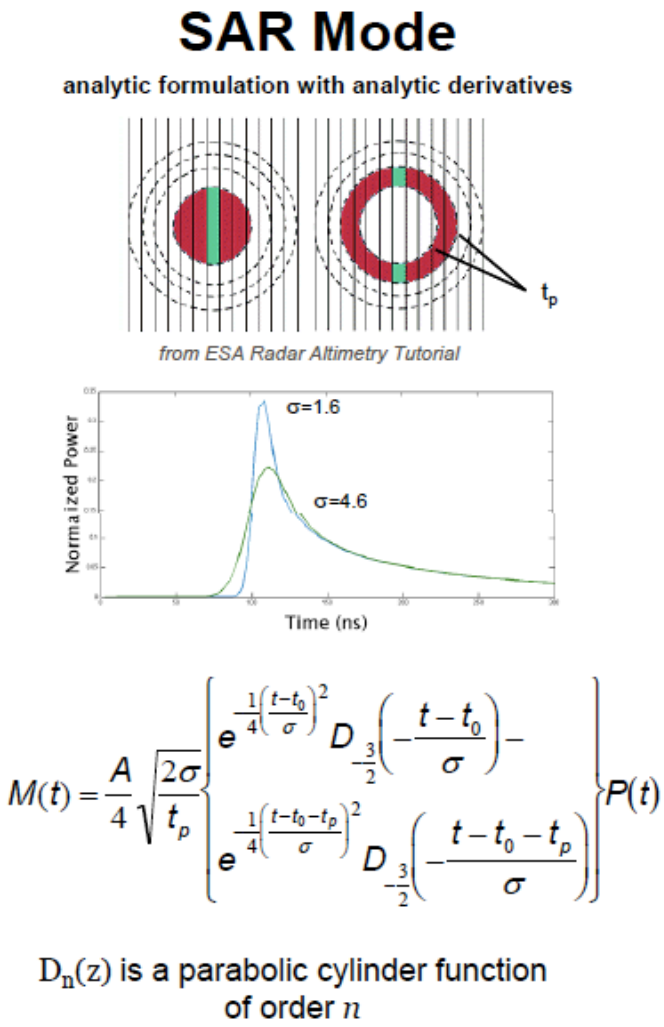

Figure 16: Formulation of the empirical SAR waveform model proposed by (Sandwell, Garcia and Smith 2011).

3.2.7. Sigma0 retrieval in SAR mode

In addition to sea surface height and significant wave height, sigma0 can also be obtained out of the altimeter radar echoes. Also referred to as backscatter coefficient, is a function of the radar frequency, polarisation and incidence angle and the target surface roughness, geometric shape and dielectric properties. It is computed from the power of the return pulse of the altimeter, and can be directly related to wind speed.

Recent studies have proved the capabilities to retrieve U10 out of sigma0 measurements from CryoSat-2 SAR waveforms. A validation exercise was conducted in the German Bight, where data between 2011 and 2012 was processed for the estimation of sea surface height, significant wave height, and the wind speed at 10 meters height (U10). Figure 17 shows the U10 winds estimated from CryoSat SAR waveforms and compared to the European Centre for Medium-Range Weather Forecasts ECMWF model. As can be seen from the figure, the high correlation between both datasets clearly shows the capabilities of this technique. For SWH of 2 meters, the precision of SAR 1 Hz wind speed was reported to be of 7 cm/s.

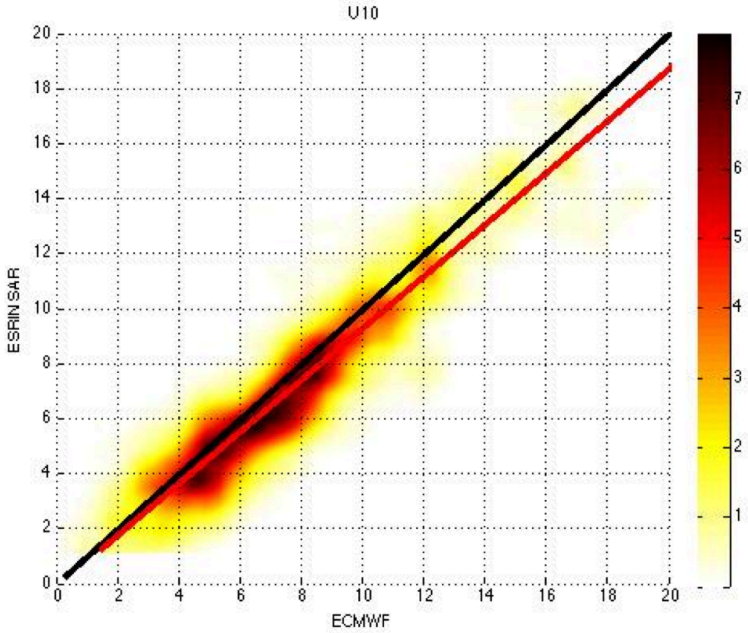

Figure 17: Scatter plot of estimated U10 wind speed from CryoSat-2 SAR data vs. ECMWF model.

3.3. RDSAR for Open Ocean

Though the SAR-mode along-track improvement in sampling resolution is straightforward, it still remains some uncertainties in the retrieved elevations as well as the other surface parameters accuracies. For example, one of main issue is to demonstrate whether, in practice, the SAR-mode height is actually better or worse than the LRM one. In addition, in order to ensure the products continuity with respect to the previous altimeter, it is necessary to derive Low Resolution Mode (LRM) waveforms from SAR Mode data. This technique is referred to as ReDuced-SAR (RDSAR) techniques, and the resulting waveforms Pseudo-LRM (or PLRM) waveforms.

To allow the assessment of the in-orbit performances of the SAR mode data and in the same manner the quality of the processing method, CNES has designed the CPP with the ability to generate and/or process two other sets of Cryosat-2 waveforms:

1) the Reduced SAR (RDSAR) mode data, aka LRM look-like or pseudo-LRM, that provide a LRM reference over the same ground tracks during SAR-mode (enabling direct comparisons of their retrievals performance), and

2) the LRM mode data to ensure that the data quality continuity between SAR and LRM measurement modes can be achieved.

Both are processed separately on-ground by the CPP facility then retracked using a similar estimator, but different geographical regions are covered from each other, one corresponding to the SAR mode locations and the other corresponding to the LRM mode areas which spread over wide ocean-spaces.

On-board the Cryosat-2 mission, SAR mode data are processed in a closed burst mode providing 4 bursts per 20-Hz tracking cycle (64 pulses at 18 kHz rhythm used in one burst). Thus when SAR data are processed in a pulse-width limited manner, the timing and number of pulses (FBR echoes) per unit time is different to the LRM sequence of a conventional altimeter (90 independent pulses regularly spaced per tracking cycle). The RDSAR method implemented in CPP consists of averaging all pulses from 4 successive SAR bursts (i.e. 4*64 = 256 FBR echoes) to form a 20 Hz Brown echo. However a much smaller number of pulses are contributing to the range noise reduction of the resulting waveform, since significant pulse-to-pulse correlations occurs at the PRF of 18 kHz (Boy, et al. 2012). Only 32 pulses, corresponding to a ~2 kHz frequency, are contributing to the speckle de-correlation instead of 90 for Cryosat-2 LRM for weak SWH, which leads to a noisy RDSAR waveforms and, thereby, a retrieved range error multiplied by a factor of sqrt(90/32) for comparison with LRM one. In practice the overall noise performance is slightly further improved since de-correlation of thermal noise occurs at higher PRF.

Prior to be averaged, each individual pulse must be shifted in the range window to be aligned on the first pulse of the cycle. The shift is computed from the vertical velocity (extracted from the COR2 altimeter command or from the orbit information). For each pulse, the range shift must be calculated taking into account the on-board altitude command already applied by the altimeter (equal to the Coarse Altitude Instruction, CAI, of the 1st pulse of each burst). So, only the Fine Altitude Instruction (FAI) must be on-ground calculated and applied to each pulse to generate the pseudo-LRM echo.

After reducing SAR mode raw data to RDSAR, an ocean retracker is applied to the RDSAR waveforms for retrieving the different geophysical parameters. This retracker consists of a conventional Brown-type ocean model with 4 parameters (SWH, epoch, Sigma0, mispointing), using least-square fitting and Gaussian wave statistics. The retrieval of the mispointing parameter is particularly appropriate to CryoSat-2 data since the satellite exhibits unstable off-nadir mispointing angle in flight. These parameters are then corrected to account for the Gaussian approximation of the PTR in the retracking algorithm scheme, the ellipticity of the CryoSat-2 antenna, and its particular speckle pattern, through pre-computed Look-Up correction Tables (LUT).

3.4. Barriers & enablers & future work for Open Oceans

Although considerable progress has been made, there is still a large amount of work to make SAR mode fully operational for the oceanographic community and to ensure continuity of high precision altimeter measurements after Jason-3 with subsequent missions (Sentinel-3 and Jason CS). In comparison with the experience the scientific community has been developing on LRM altimetry for decades (20 years since the first TP and ERS waveforms and much more since skylab, seasat and geosat-1), SAR mode processors are still in their infancy. Recent investigations led by agencies and research groups concerned by SAR mode technology (e.g., ESA, SAMOSA group, Thales Alenia Space, UCL, CNES, CLS, NOAA, …) have already produced very good preliminary results for CryoSat-2 SAR waveforms, with the development of robust retrackers (based on analytical or numerical algorithm consideration) that are suited to the SAR echoes. However, this work is still on going, as retrackers have not yet succeeded retrieving together high-resolution sea surface heights, wave heights and wind speeds from SAR-mode data.

Some remaining issues that may impact the SAR-mode performance still need to be analyzed and worked out, namely:

- the inconsistent behaviour of SAR retracker at low wave heights (below 1m) currently observed by all the teams involved in SAR processing,
- the sensitivity of the SAR mode retrievals to varying orbital and instrumental parameters, such as the platform mispointing angles, the altitude, the spacecraft velocity,
- the potential impact of the long-wavelength swell waves (close to the along-track SAR resolution) on the estimates,
- the lack of SSB solution suitable to SAR mode measurement geometry. Similarly to the conventional altimeter approach, the SSB for the SAR mode shall be empirically evaluated from altimeter itself, as function of wave height and backscatter coefficient measurements, since theoretical electromagnetic bias models are not accurate enough. At this moment, one limitation of this method may reside in the difficulty to estimate SAR mode sigma-naught for peaky waveforms and then to derive any SAR SSB correction (unless RDSAR estimate is used in the absence of SAR sigma-naught). Furthermore, we remind that trying to estimate an empirical SSB correction is relatively complicated since it must be constructed over many cycles (allowing to account for seasonal variations) to make the model consistent throughout a mission.

4. Coastal Zones

During the last two decades, satellite altimetry has provided accurate measurements of the sea surface height, significant wave height and wind speeds over the oceans. There is, however, an increasing demand to extend these observations as close to the coast as possible. Some limitations inherent to the conventional technique jeopardize the use of altimeter data for most coastal applications. Indeed, issues of land contamination in the footprint have typically resulted in flagging and rejection of data. A number of studies have analysed this problem and some initiatives have been launched for an extensive reprocessing of the coastal altimetric data with new, specifically tailored algorithms, provided their great value for a wide variety of coastal applications.

The scientific and social relevance of this branch of altimetry triggered the organisation of yearly international workshops, the Coastal Altimetry Workshops, that have been celebrated every year and that will reach, in 2013, the 7th edition (for more information visit www.coastalt.eu).

4.1. SAR-Altimetry for Coastal Areas

The increasing interest of SAR mode altimetry, especially in coastal areas, is linked to the higher resolving measurement capability in the direction of the platform velocity, i.e. along-track direction. The improved resolution is a consequence of the delay-Doppler processing of the radar echoes. The along-track resolution reaches values typically around 250 to 300 meters (R. K. Raney, Resolution and Precision of a Delay-Doppler Radar Altimeter 2005), which represents a remarkable improvement in comparison to the several kilometres currently achieved with conventional altimetry. In addition, due to the coherent processing of the received radar echoes, the final signal-to-noise ratio (SNR) of the system is increased by around 10 dB, which results in an improvement of the sea surface height (SSH), significant wave height (SWH) and wind speed (WS) estimation. Figure 18 shows a plot of height precision versus SWH for a delay-Doppler altimeter and a conventional radar altimeter. The plot shows that a DDA is significantly better in precision than a conventional radar altimeter (RA) (R. K. Raney, Resolution and Precision of a Delay-Doppler Radar Altimeter 2005). The figure also shows that height measurements from a delay-Doppler altimeter are degraded less than those from a conventional radar altimeter in response to increasing SWH.

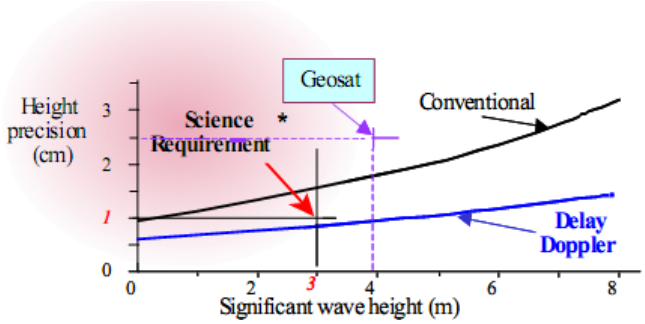

Figure 18: Sea Surface Height precision as a function of the Significant Wave Height, for a conventional and delay-Doppler altimeter (R. K. Raney, Resolution and Precision of a Delay-Doppler Radar Altimeter 2005).

The shrinking of the radar footprint allows reducing the land contamination effect, which is the main limitation in the use of satellite altimetry for coastal areas. As a consequence of this, SSH, SWH, and WS measurements are expected to be provided at as close as several hundred meters from the shore. Various studies have already shown the capabilities of a delay-Doppler Altimeter to obtain useful radar echoes at a distance about 300 meters from the coast: see, for example, (J Benveniste 2012). As can be observed in Figure 19 waveform #1854, obtained from few hundred meters from the coast, was successfully retracked by the SAMOSA model, which allowed estimating the range delay and SWH for that area. However, this lower bound when approaching to the coast is not always reachable. This is explained further in the next subsection.

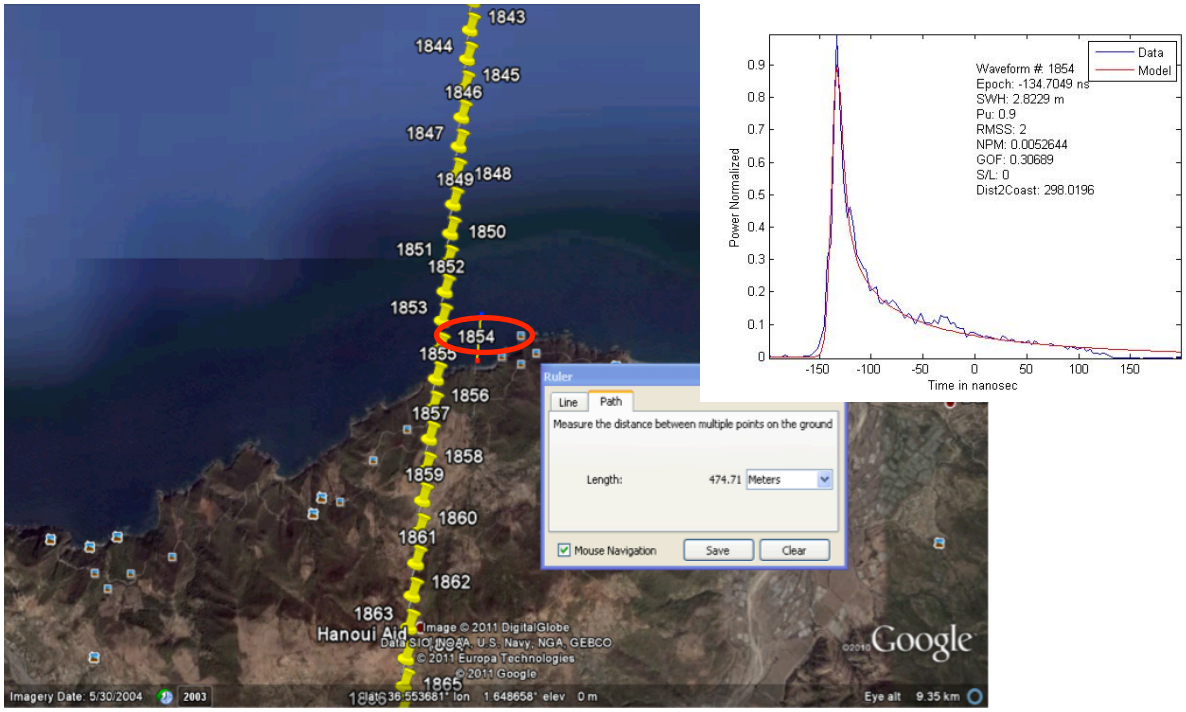

Figure 19: Example of SAR Altimetry waveforms for a satellite track perpendicular to the coast.

Next sections review the effects of the combined response of land and ocean in the coastal regions, the processing algorithms that are currently being used, and the necessary corrections to extract meaningful information from altimeter data for coastal regions.

4.2. Land Contamination Effects

The effects of the contamination of land scattering on the radar altimeter echoes near the coast depend on the relative weight of the power coming from the land and the ocean. If the land surface scattering is much lower than the ocean's one the waveforms will be slightly affected, whereas if the coastline is very bright, i.e., flat and wet such as on coral reefs, a strong coherent component is expected to arise from these areas, which will highly distort the well known ocean-like waveform shape on which retrackers are designed to work. It is clear then that the geometry and characteristics of the coastline will contribute to define the shape of the waveform, thus creating a vast number of possibilities for waveform shapes. Examples of these types of waveforms are shown in Figure 20.

The effect of land contamination on the altimeter waveforms can also be readily observed in Figure 21, from, (Deng 2003). In this case, a single bright scatterer was introduced on a simulated homogeneous scenario. As can be observed, a hyperbola appears on the waveforms due to the relative position of the altimeter and the scatterer on the surface. As the altimeter moves along-track towards the scatterer, the range between the satellite and the target is reduced according to a quadratic relationship, thus the bins of the waveform affected by the bright scatterer change until the sub-satellite position coincides with the bright scatterer position, i.e., the minimum range situation between altimeter and point scatterer. In the same way, a patch of reduced scattering could also produce similar effects on the final waveforms.

The combination of the effects of several scatterers with different backscattering intensities on the surface can lead to random variations of the waveforms along time, (Graham, Cipollini and Thibaut 2012), which prevents the application of conventional Brown retracking techniques to retrieve geophysical parameters from altimeter data.

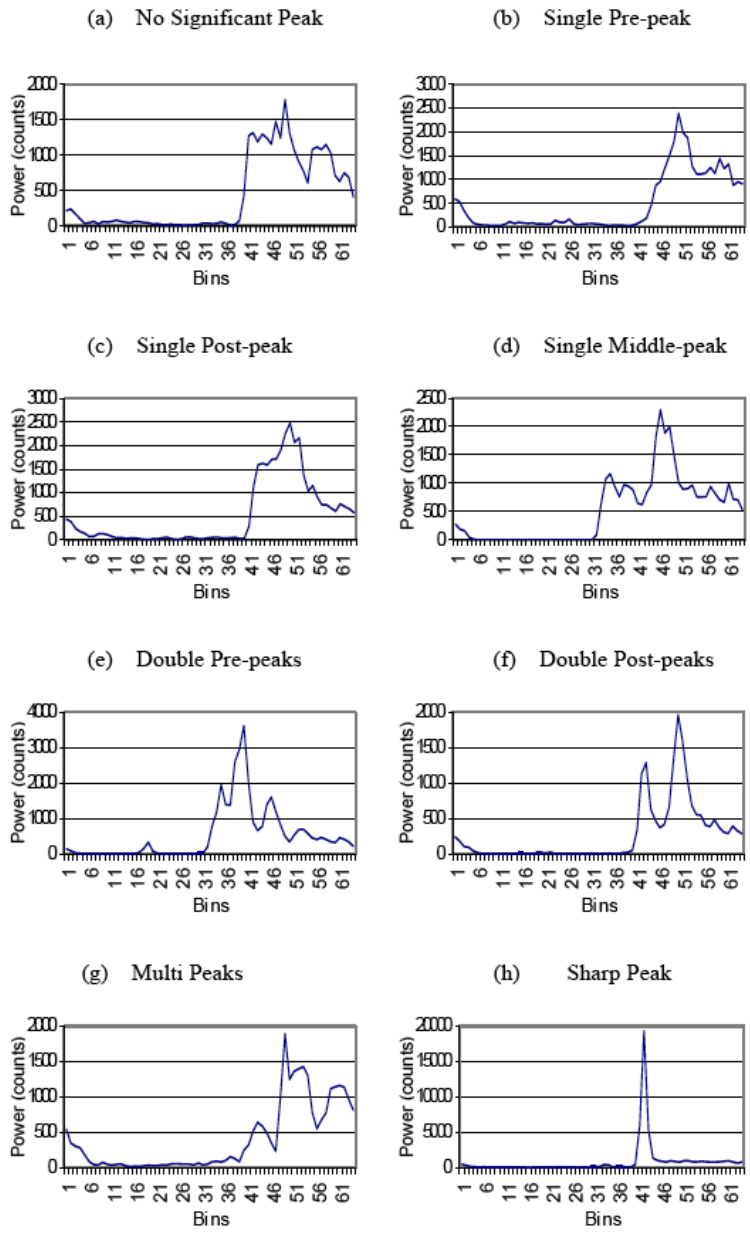

Figure 20: Typical ERS2 waveform categories in Australian coasts (Deng 2003).

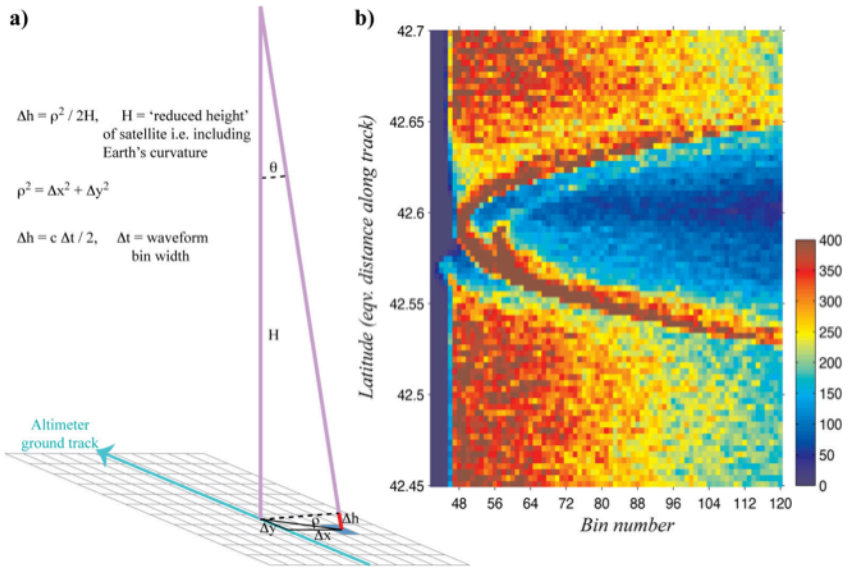

Figure 21: a) Schematic representation of the scattering geometry. The point of minimum distance to the altimeter corresponds to the sub-satellite point. The distance of a single scatterer with respect to the altimeter varies along time as shown in panel b); (Quartly 2011).

As pointed out above, in a delay-Doppler altimeter the resolution improvement occurs only on the along-track direction, while the across-track direction remains pulse-limited. The result is an elongated footprint, as shown in Figure 13, perpendicular to the satellite flight direction. This implies that the DDA's response in coastal regions depends on the relative orientation between the coastline and the spacecraft orbital plane (Raney and Phalippou 2011). The 250 m dimension prevails when the coastlines are perpendicular the flight direction, whereas the longer pulse-limited direction domintaes when the altimeter is passing parallel to the shore.

In (Dinardo, Lucas and Benveniste 2011) the authors provided examples of CryoSat-2 SAR mode waveforms contaminated by land effect. As can be observed in Figure 22, despite the fact that the distance to the coast is almost 5 km, SAR waveform #56 is corrupted by a land effect in its tail, which prevents the use of this data for oceanographic applicatons.

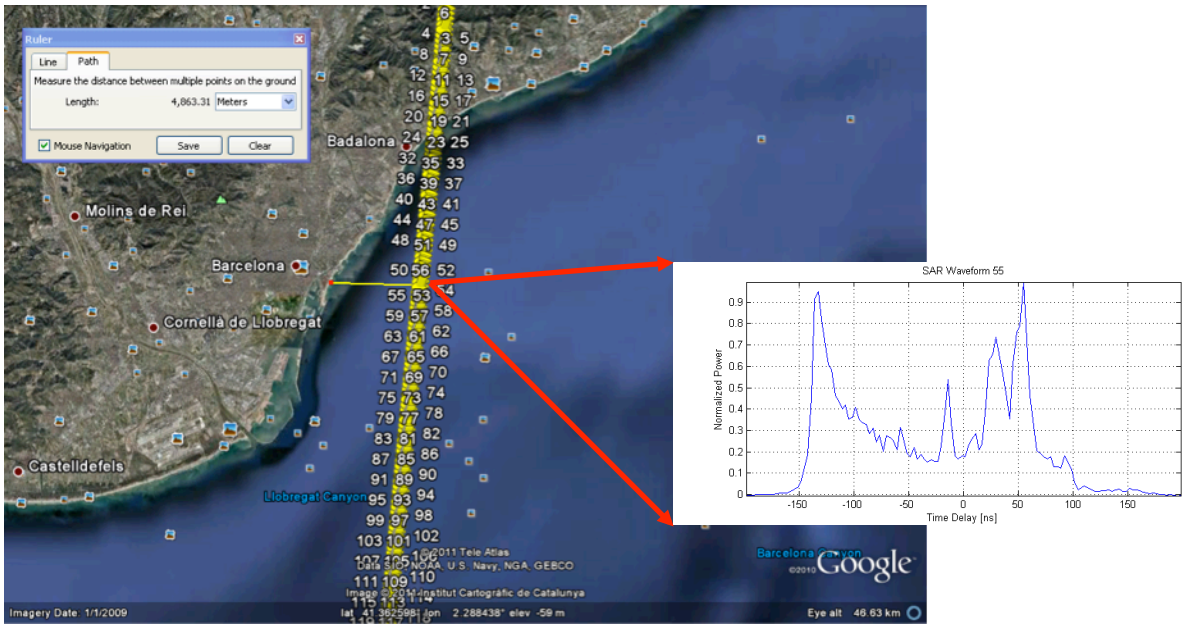

Figure 22: Example of SAR Altimetry waveforms for a satellite track parallel to the coast.

4.3. Technology Status, Retracking Techniques

Several initiatives such as the PISTACH and COASTALT projects have investigated the effects of the contamination of land reflections on the radar altimeter echoes near the coast, and have proposed suitable technological solutions for the analysis of such data.

A solution proposed within the COASTALT project was the pre-processing of the land contaminated altimeter waveforms, the so called "Hyperbolic pretracker" (Quartly 2011), in order to eliminate the possible effect of land scattering. This algorithm is used to locate and remove hyperbolic feature within the 2-D waveform data. The resultant cleaned waveforms are then more suitable for conventional Brown-oceanic retracking models. However, the technique did not manage to restore the full Brown-like waveforms out of the contaminated data due to variations in the altimeter Automatic Gain Control (AGC) and tracker window.

Other techniques based on waveform retracking have also been used to analyse altimeter data near the coast. The retracking process is essentially a statistical minimization process in which a model is fitted to the data. The most common ways of data fitting within altimetry are the Maximum Likelihood Estimation (MLE) and the Least Square Estimation Methods (LSE).
During the COASTALT project a physically based processing retracking technique was developed according to the shape of the waveform. In this processing algorithm, three different retrackers work in parallel. These are (Gommenginger, et al. 2011):

- Conventional Brown Ocean Retracker: for ocean like waveforms.
- The Beta-parameter retracker with Exponential trailing edge (Deng 2003): This waveform model is well suited to fit high intensity peaky waveforms, with a rapidly decaying trailing edge.
- A semi-empirical, Mixed Brown-Specular Retracker consisting of the superposition of a Brown ocean waveform and one or more Beg-retracker specular echoes.

In the same way, within the PISTACH project, a retracking technique based on the Jason-2 retracking scheme was implemented and tested. This retracking technique is based on the estimation of the sea surface height and significant wave height for waveforms bins that are not affected by land contaminations, that is, the bins on the trailing edge of the waveform. The results obtained showed that it was possible to estimate both SSH and SWH closer to the coast than with conventional retrackers.

In order to finally estimate geophysical products from altimeter data certain corrections need to be applied to the parameters obtained from the retracker. In the case of coastal zones these corrections are not always available due to the limitations for providing these data with the required spatial and temporal resolution. In addition, some of these corrections are inherent of coastal areas, and are not usually provided for open ocean data corrections. Those are reviewed in the next section.

4.4. Corrections in Coastal Areas

Apart from the conventional correction applied in open-ocean altimetry, the wet tropospheric correction is, together with the tidal correction, one of the two largest obstacles for deriving good altimetric estimates over coastal regions (Quartly 2011), (Andersen and Scharroo 2011).

The former is affected by a complete absence of measurements along a strip of few tens of kilometres from the coast. The reason for this is that the radiometer measurements, which are usually used to measure water vapour, are severely affected by land contamination due to the difference in emissivity of land and water, (Obligis, et al. 2011). This extends for the whole footprint of the radiometer. The options to mitigate this effect are: to model the correction from some atmospheric model, such as ECMWF, by ensuring continuity of the radiometer measurements and the model to model and remove the influence of land contamination in the data, (Obligis, et al. 2011); or to estimate the Zenith Tropospheric Delay and Integrated Water Vapour by GPS permanent observation networks (Fernandes, et al. Jul 2010). Different institutions around Europe are currently investigating all these approaches.

Regarding the tide correction, the issue is the accuracy of the correction based on global models, as these models are prone to large errors in the coastal zones. Bathymetry errors and inaccurate lateral boundary information can lead to errors in the total elevation of water predicted by the

models. In addition, the limited spatial resolution of models, and the temporal variability of these parameters can lead to further errors. Regional models could provide a good estimation of tides for specific regions; however, the problem here is the continuity of these models with the more global and deep ocean tide models.

4.5. Conclusions and Considerations for Further Work

As mentioned above, SAR altimetry is expected to provide improved precision and resolution products along the satellite track, thus improving the estimation of coastal zone phenomena. However, the resolution across-track is not improved, as there is not an additional Doppler bandwidth due to the platform movement. These aspect and the specificities of the data processing will need to be considered in depth during the LOTUS project. The use of uncompressed SAR mode data could be of great benefit in conjunction with Digital Elevation Models in order to identify land contamination effects. In addition, the different corrections specific for coastal areas will need to be deeply investigated in order to provide useful products as close to the coast as possible.

5. Polar Ocean

The observation of the sea surface height (SSH) in the Polar Oceans has previously been performed from conventional radar altimetry in order to estimate the Arctic sea ice volume.

5.1. Identifying sea surface radar returns in sea ice covered regions

The waveforms returned from an ice covered ocean shows a high variability in shape depending on the sea ice type and the fraction of open water within the footprint. Before the SSH can be derived the radar observations needs to be separated into measurements of sea ice floes, sea ice leads and unknowns. It is possible to make this separation based on the returned waveform characteristics, since the sea ice leads will behave like a specular target whereas the sea ice floes will behave more like a diffuse target. A specular reflection is possible if more than 1% of the footprint satisfies the Rayleigh criterion (Drinkwater 1991).

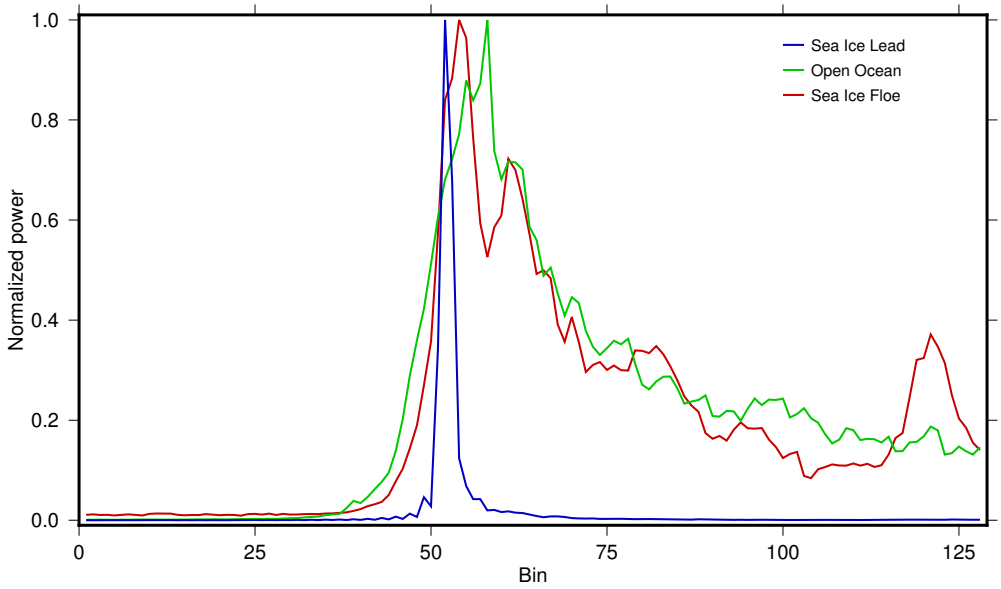

Figure 23: Examples of three CryoSat-2 SAR waveforms from the Barents Sea on March 15 2013. Note that the Open Ocean waveform could be contaminated by sea ice debris.

In the following two parameters to characterize and classify the radar waveforms will be described.

5.1.1. Pulse Peakiness (PP)

For a conventional altimeter (e.g. ERS-1/2 or ENVISAT) the separation of return waveforms, into sea ice leads and sea ice floes, can be performed using the pulse peakiness parameter (see Equation 1). The PP parameter is defined as the maximal sampled power scaled by a constant and divided by the summed power of all useable samples in the waveform and thus indicates how spiky the main return of the waveform is.

$$PP = \frac{30 \cdot P_{\max}}{\sum P_i}$$

Equation 1: Pulse Peakiness for SeaSat, as defined in (Laxon og Rapley 1987).

In the formulation by (Laxon og Rapley 1987) the scaling constant was selected to give a PP value around 1 for SeaSat ocean returns. Later formulations of the peakiness uses different scaling constants adapted to the individual characteristics of the radar instruments used in the studies, or using a scaling of unity.

In the version 2.4 release of the CryoSat-2 L2 data a pulse peakiness is calculated and supplied by ESA. The scaling used by ESA is somewhat different with a ocean value around 50 and values up to 550.

5.1.2. Stack Standard Deviation (SSD)

For a SAR altimeter it is furthermore possible to describe the reflecting properties of the surface. This is possible as the multi-looked SAR waveform is composed of a number of beams illuminating the surface under a range of different incident angles.

Figure 2 is an illustration of the power reflected from a sea ice floe acting as a diffuse reflecting surface. For a perfect diffuse reflector the energy from a radar beam will be spread uniformly in all directions and the shape of the returned power as a function of look angle will be similar to the two way antenna pattern.

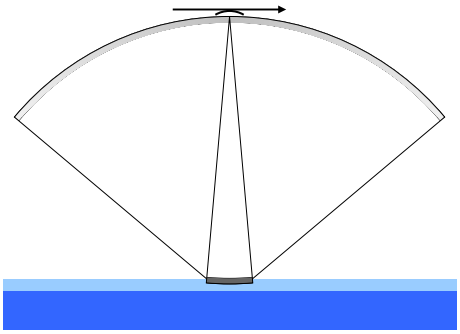

Figure 24: Power reflected from a diffuse surface (e.g. a sea ice floe) as function of look angle will primarily be affected by the antenna pattern.

A specular reflecting surface will act as a mirror, where the majority of the power will be reflected at an angle equal to the incident angle, see Figure 25.

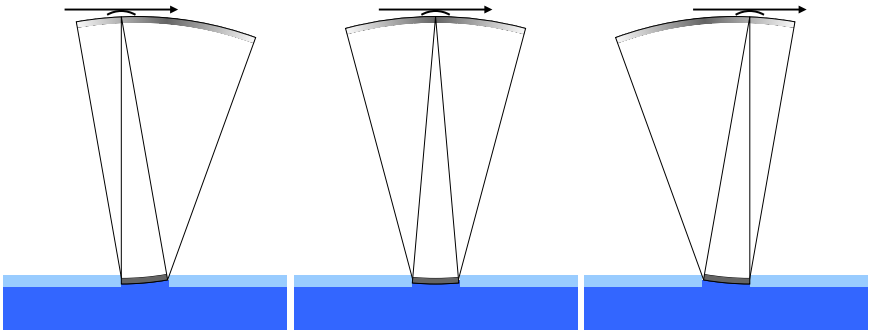

Figure 25: Returned power from a specular reflection sea ice lead during an overpass. During approach the energy will be reflected forward (left), when over the lead it will be returned to the radar antenna (middle) and when departing it will be reflected backwards (right).

A simulation of the return power as a function of the look angle, also called the stack, for a diffuse and a semi specular reflecting surface is presented in Figure 26. In the ESA processing of CryoSat-2 SAR data a Gaussian is fitted to the stack and the center, standard deviation, skewness, and kurtosis of the fit is provided in the product.

In (Laxon, Giles, et al. 2013) the SSD is introduced as a supplement to the PP for the classification of sea ice leads and sea ice floes in the Arctic Ocean.

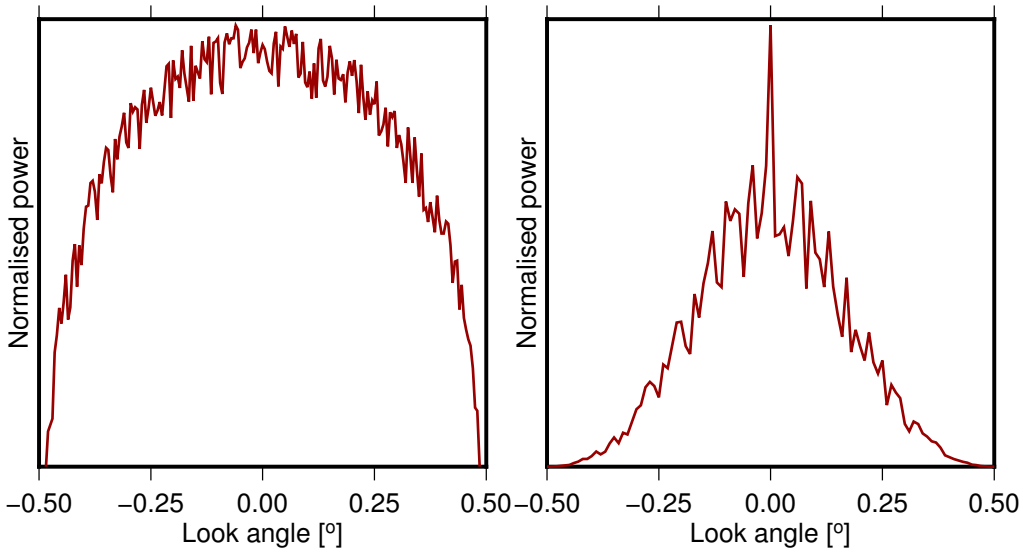

Figure 26: Simulated return power in a SAR altimeter stack as a function of look angle from a uniform rough surface (left) and a surface with a specular component (right). Adapted from (Wingham, Francis og Baker, CryoSat: A mission to determine the fluctuations in Earth's land and marine ice fields 2006).

5.1.3.Classification of returns in sea ice covered regions

Due to the limited period of SAR altimetry data over sea ice covered regions, only few studies of classifications schemes has been carried out, (Boy, et al. 2012), (Gommenginger, et al. 2011).

An investigation of the ESA L2 product shows that the classification of returns in sea ice covered areas are based on the pulse peakiness and stack standard deviation, see Figure 27. In the ESA L2 product a return is flagged as sea ice lead if the PP is equal to or higher than 300 and the SSD is 3 or smaller. Sea ice floes are flagged if the PP is 160 or smaller and have a SSD of 3 or smaller. The separation between open ocean, also include in Figure 28, and sea ice covered areas is based on a geographical mask derived primarily from passive microwave data.

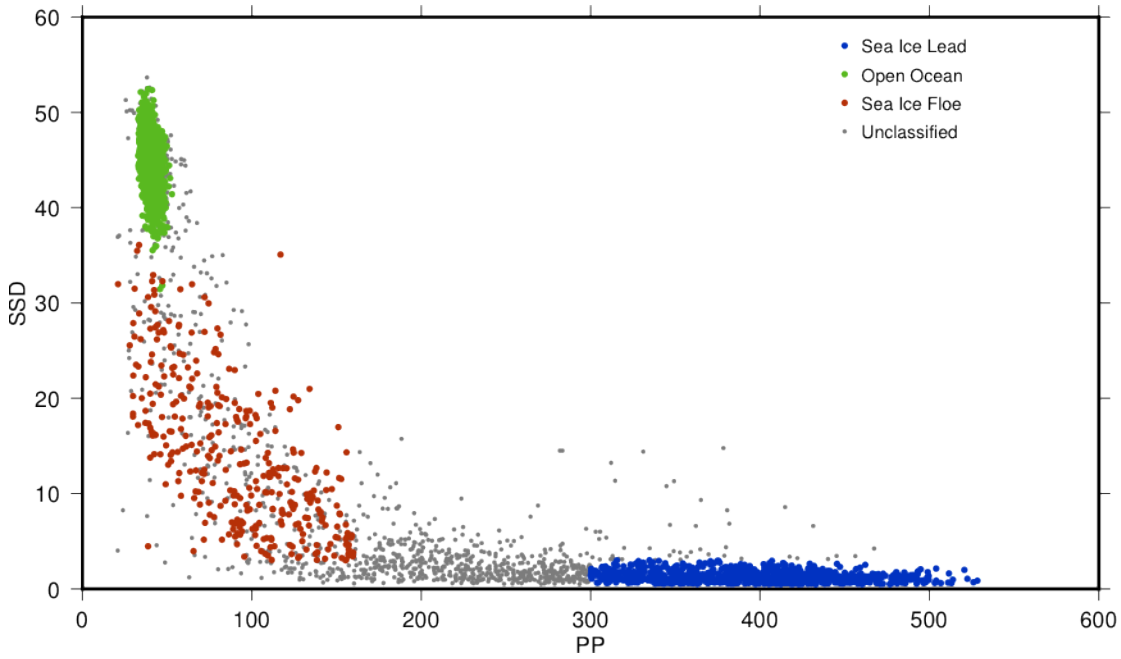

Figure 27: ESA classification of a CryoSat-2 track crossing the Barents Sea on March 15 2013.

In a resent study by (Laxon, Giles, et al. 2013) the classification is based on PP and SSD. Using a standard scaling of the PP they classify returns as sea ice leads if PP is greater than 18 and SSD smaller than 4 and as sea ice floes if PP is less than 9 and SSD greater than 4.

5.2. Retracking specular waveforms

Retracking of specular waveforms is challenging since almost all power is concentrated in a few range samples and it is therefore often not possible to fit a physical model to the waveform. Instead simple empirical retrackers (e.g. threshold retrackers) have been used on conventional altimetry data.

The introduction of SAR processing on the CryoSat-2 data made the waveform even steeper. The steep leading edge and narrow peak meant that the peak were poorly represented in the product. To address the poor representation of the peak the baseline B processing (February 1st 2012 and later) of CryoSat-2 data uses a factor 2 oversampling of the waveform resulting in an apparent doubling of the range resolution (ESA og UCL 2013).

In the study by the waveforms are retracked with a model composed by a Gaussian and an exponential decaying function (Laxon, Giles, et al. 2013) and (Giles, et al. 2007).

The LARS radar processor at DTU Space has a number of retrackers including a threshold retracker for specular targets and a prototype of the retracker presented in (Giles, et al. 2007).

5.3. Available polar ocean SAR altimetry products

The ESA L2 CryoSat-2 product is one of the few widely available retracked SAR altimetry products. Figure 29 shows the sea ice lead height relative to the UCL04 mean sea surface (MSS) for March 2013, both quantities are part of the ESA L2 CryoSat-2 product. There is a clear discontinuity in the variability around 81.5 degrees North above which the variability is significantly larger than for the rest of the Arctic Ocean. This discontinuity arises because UCL04 is a hybrid model where 81.5 degrees North indicates the shift from ERS MSS to a combination of the Arctic Gravity Project Geoid and PIMS Mean Dynamic Topography.

Instead the ESA L2 sea ice lead heights are compared to the DTU10 MSS, see Figure 30. The agreement between the ESA L2 sea ice lead heights and the MSS is greatly improved, but some small scale differences is still seen close to the North Pole and some larger scale differences in the Beaufort Sea, the Barents Sea and the Laptev Sea. One month of data is however far from sufficient for a proper evaluation of the ESA L2 product.

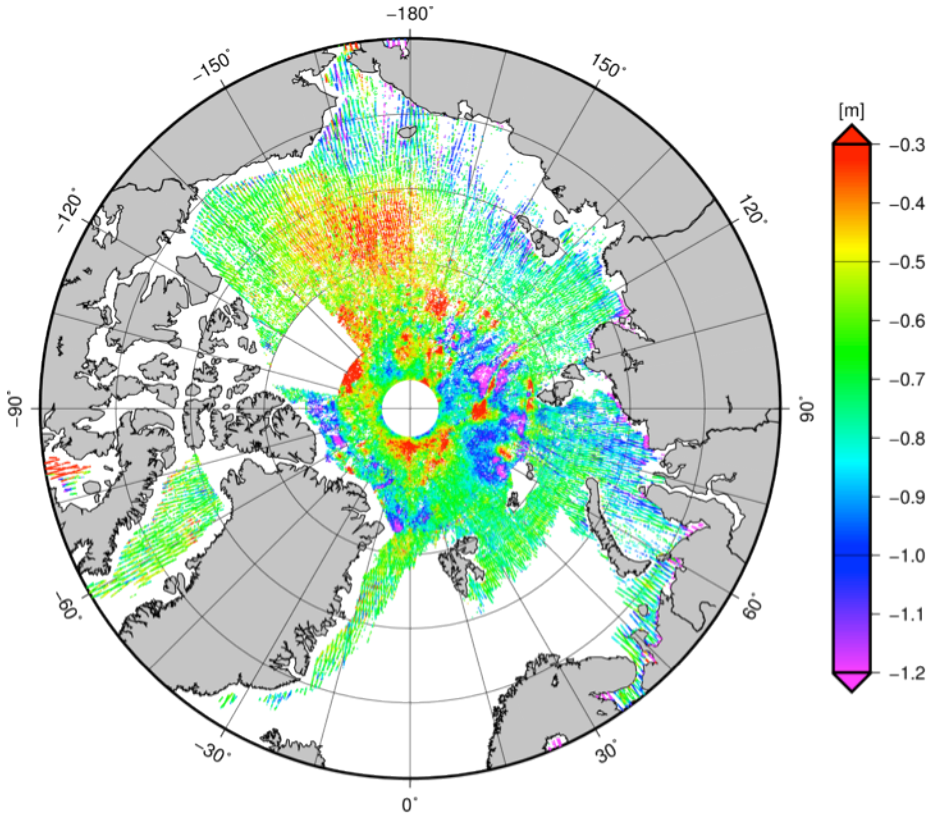

Figure 28: Heights of sea ice leads in March 2013 relative to the UCL04 MSS, both part of the ESA L2 product.

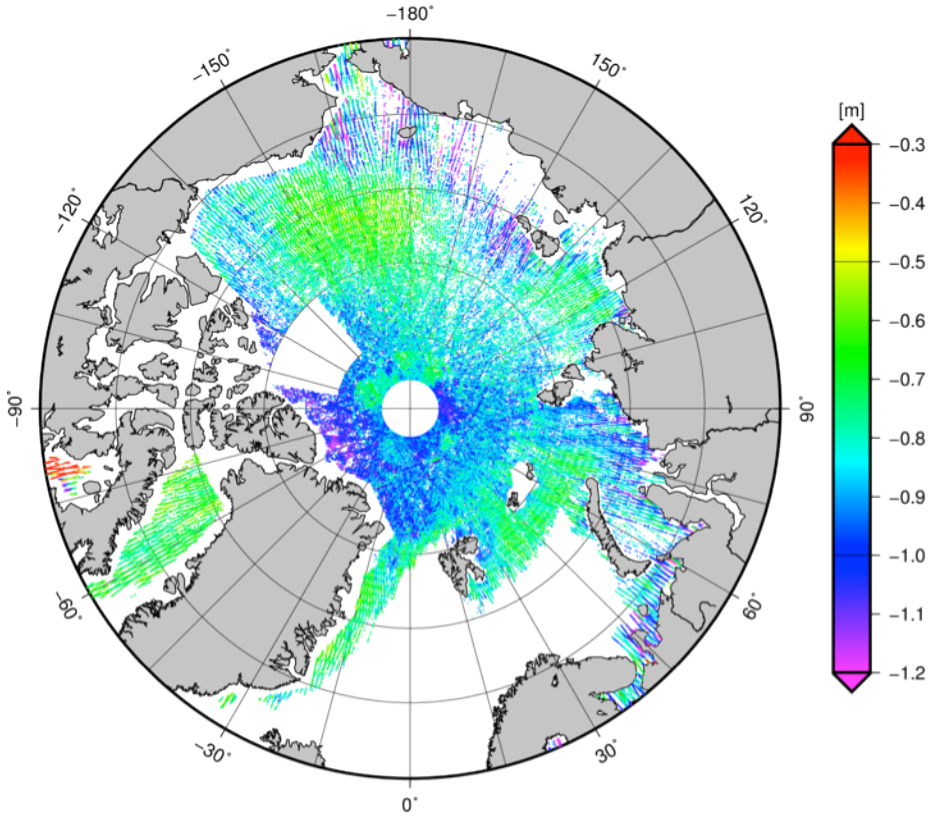

Figure 29: Heights of sea ice leads in March 2013 relative to the DTU10 MSS.

6. Bibliography

A. Halimi, C. Mailhes, J-Y. Tourneret, F. Boy, N. Picot, and P. Thibaut. *An analytical model for Doppler altimetry and its estimation algorithm.* 2012.

Andersen, O. B., and R. Scharro. *Range and Geophsyical Corrections in Coastal Regions: And Implications for Mean Sea Surface Determination - Coastal Altimetry, Chapter 5.* Edited by Stefano and Kostianoy, Andrey G. and Cipollini, Paolo and Benveniste, Jérôme Vignudelli. Springer, 2011.

Boy, F., et al. *Cryosat Processing Prototype, LRM and SAR Processing.* Edited by presented at the 2012 Ocean Surface Topography Science Team Meeting. Available online: http://www.aviso.oceanobs.com/fileadmin/documents/OSTST/2012/oral/02_friday_28/02_instr_processing_II/02_IP2_Boy.pdf. 2012.

Brown, G.S. *The Average Impulse Response of a Rough Surface and its Applications.* Vols. AP-25. IEEE Trans Antennas Propagation, 1977.

ESA, ESRIN, and MSSL UCL. "CryoSat Product Handbook, April 2013." ESRIN - ESA and Mullard Space Science Laboratory - University College London, 2013.

Deng, Xiaoli. *Improvement of Geodetic Parameter Estimation in Coasta Regions from Satellite Radar Altimetry.* PhD Thesis, Curtin University of Technology, 2003.

Dinardo, S., B. Lucas, and J. Benveniste. *SAR Altimetry in Coastal Zone: Performances, Limits, Perspectives.* San Diego: 5th Coastal Altimetry Workshop, 2011.

Drinkwater, Mark. "Ku band airborne radar altimeter observations of marginal sea ice during the 1984 Marginal Ice Zone Experiment." *Journal of Geophysical Research*, 1991: 4555-4572.

Fu, L-L., and A.Cazenave. *Satellite Altimetry and Earth Science.* Vol. 69. Academic Press, International Geophysics Series, 2001.

Fernandes, M.J., C. Lazaro, A.L. Nunes, N. Pires, L. Bastos, and V.B. Mendes. *GNSS-Derived Path Delay: An Approach to Compute the Wet Tropospheric Correction for Coastal Altimetry.* Vol. 7. Geoscience and Remote Sensing Letters, IEEE, Jul 2010.

Giles, K. , D. J. Wingham, N. Galin, and R. Cullen. *Precise estimates of ocean surface parameters from CryoSat.* Venice: OST Science Team meeting, 2012.

Giles, K. A., et al. "Combined Airborne Laser and Radar Altimeter Measurements Over the Fram Strait in May 2002." *Remote Sensing of Environment* 11 (2007): 182-194.

Gommenginger, C., et al. *Retracking Altimeter Waveforms Near the Coasts - Coastal Altimetry, chapter 4.* Edited by S. Vignudelli, A. G. Kostianoy, P. Cipollini and J. Benveniste. Springer, 2011.

Graham, Quartly, Paolo Cipollini, and Pierre Thibaut. *Seamless transition from ocean to coastal retracking algorithms.* San Diego: OSTST Meeting, 2012.

J Benveniste, P Cipollini, C Gommenginger, C Martin-Puig, D Cotton, S Dinardo. *Road-mapping the Way Forward for Sentinel-3 Topography Mission SAR-Mode waveform Re-tracking over water surfaces.* Mysore: 39th COSPAR Scientific Assembly, 2012.

Laxon, S. W., and C. G. Rapley. "Radar altimeter data quality flagging." *Advances in Space Research* 7, no. 11 (1987): 315-318.

Laxon, S. W., et al. "CryoSat-2 estimates of Arctic sea ice thickness and volume." *Geophysical Research Letters* 40 (2013): 732-737.

Laxon, S. "Sea ice extent mapping using the ERS-1 radar altimeter." *Advances in Remote Sensensing* 3 (1994): 112–116.

Obligis, E., C. Desportes, L. Eymard, M. J. Fernandes, C. Lázaro, and A. L. Nunes. *Tropospheric Corrections for Coastal Altimetry.* Edited by Stefano Vignudelli, Andrey G. Kostianoy, Paolo Cipollini and Jérôme Benveniste. Springer, 2011.

Quartly, Graham. *Development and Implementation of the Hyperbolic Pretracker.* COASTALT-2 project Deliverable D3.3, 2011.

Peacock, Neil R., and Seymour W. Laxon. "Sea surface height determination in the Arctic Ocean from ERS altimetry." *Journal of Geophysical Research*, 2004.

Phalippou, L., and and V. Enjolras. *Re-Tracking of SAR Altimeter Ocean Power-Waveforms and Related Accuracies of the Retrieved Sea Surface Height, Significant Wave Height and Wind Speed.* Barcelona: Proc. IEEE IGARSS, 2007.

Sandwell, D.T. , E. Garcia, and W.H.F. Smith. *Improved Marine Gravity from CryoSat and Jason-1.* San Diego: OST Science Team meeting, 2011.

SAMOSA Team. *State of the Art Assessment (WP1) Version 1.0.* available in: http://www.satoc.eu/projects/samosa/docs/SAMOSA-TN01-V1.0full.pdf, 2008.

Ray, C., and C Martin-Puig. *SAMOSA models trade-off technical note. D1 SAMOSA-3 project, WP2100.* 2012.

Raney, Keith. *The delay Doppler radar altimeter.* Vol. 36(5). IEEE Transaction in Geoscience and Remote Sensing, 1998.

Raney, R. K. *Resolution and Precision of a Delay-Doppler Radar Altimeter.* Vol. 3. OCEANS, 2005. Proceedings of MTS/IEEE , 2005.

Raney, R. K., and L. - Coastal Altimetry, Chapter 20 Phalippou. *The Future of Coastal Altimetry.* Edited by A. G. Kostianoy, P. Cipollini, J. Benveniste S. Vignudelli. Springer, 2011.

Wingham, D. J., C. R. Francis, and S. Baker. "CryoSat: A mission to determine the fluctuations in Earth's land and marine ice fields." *Advances in Space Research*, 2006: 841-871.

Wingham, D. J., L. Phalippou, C. Mavrocordatos, and D Wallis. *The Mean Echo and Echo Cross Product From a Beamforming Interferometric Altimeter and Their Application to Elevation Measurement.* Vol. 42. IEEE Transactions on Geoscience and Remote Sensing, 2004.